Multi-elemental and Strontium-Neodymium Isotopic Signatures in Charred Wood: Potential for Wood Provenance Studies

Anna Imbert Štulc, Anne Poszwa, Stéphane Ponton, Jean-Luc Dupouey, Julien Bouchez, Jérémie Bardin, Frédéric Delarue, Sylvie Coubray, Michel Lemoine, Christophe Rose, et al.

BRILL

INTERNATIONAL JOURNAL OF WOOD CULTURE
3 (2023) 1–48

The International Journal of Wood Culture
brill.com/ijwc

Multi-elemental and Strontium-Neodymium Isotopic Signatures in Charred Wood: Potential for Wood Provenance Studies

Anna Imbert Štulc | ORCID: 0000-0002-3833-9195
AASPE UMR 7209 (CNRS-MNHN), Muséum national d'Histoire naturelle, Paris, France
Corresponding author
anna.stulcova@mnhn.fr

Anne Poszwa | ORCID: 0000-0001-6133-3130
LIEC UMR 7360 (Université de Lorraine-CNRS), Nancy, France
anne.poszwa@univ-lorraine.fr

Stéphane Ponton | ORCID: 0000-0002-4821-2438
SILVA UMR 1434 (INRAE) Université de Lorraine, AgroParisTech, INRAE, Nancy, France
stephane.ponton@inrae.fr

Jean-Luc Dupouey | ORCID: 0000-0002-7396-8691
SILVA UMR 1434 (INRAE) Université de Lorraine, AgroParisTech, INRAE, Nancy, France
jean-luc.dupouey@inrae.fr

Julien Bouchez | ORCID: 0000-0003-4832-1615
Institut de physique du globe de Paris (Université de Paris Cité, CNRS), Paris, France
bouchez@ipgp.fr

Jérémie Bardin | ORCID: 0000-0003-2382-4259
CR2P UMR 7207 (Sorbonne Université, MNHN, CNRS), Paris, France
jeremie.bardin@sorbonne-universite.fr

Frédéric Delarue | ORCID: 0000-0001-7054-612X
METIS UMR 7619 (CNRS, EPHE, PSL), Sorbonne Université, Paris, France
frederic.delarue@upmc.fr

Sylvie Coubray | ORCID: 0000-0001-7650-2195
Inrap, Centre – Île-de-France, 93694 Pantin, France
sylvie.coubray@inrap.fr

Michel Lemoine
AASPE UMR 7209 (CNRS-MNHN), Muséum national d'Histoire naturelle, Paris, France
mlemoine@mnhn.fr

Christophe Rose
SILVA UMR 1434 (INRAE) Université de Lorraine, AgroParisTech, INRAE, Nancy, France
christophe.rose@inrae.fr

Julien Ruelle | ORCID: 0000-0001-8780-5650
SILVA UMR 1434 (INRAE) Université de Lorraine, AgroParisTech, INRAE, Nancy, France
julien.ruelle@inrae.fr

Maximilien Beuret | ORCID: 0000-0002-4327-5747
LIEC UMR 7360 (Université de Lorraine-CNRS), Nancy, France
maximilien.beuret@univ-lorraine.fr

Thanh Thuy Nguyen Tu | ORCID: 0000-0003-1543-4998
METIS UMR 7619 (CNRS, EPHE, PSL), Sorbonne Université, Paris, France
thanh-thuy.nguyen_tu@upmc.fr

Alexa Dufraisse | ORCID: 0000-0002-2496-8644
AASPE UMR 7209 (CNRS-MNHN), Muséum national d'Histoire naturelle, Paris, France
alexa.dufraisse@mnhn.fr

Abstract

The chemical composition of the wood reflects the composition of the soil over which the corresponding tree has developed. Multi-elemental and isotopic signatures, which are characteristic of the soil and underlying rock substrates, are potentially powerful tools for determining wood provenance. These tracers are of special interest for charred archaeological wood because they circumvent some limitations of dendrochronological provenancing linked to tree-ring loss. However, thermal degradation may introduce a significant bias in wood chemical and isotopic analyses. This experimental study focused on the effects of carbonization temperature on three geochemical wood markers: elemental signatures and isotopic signatures of strontium and neodymium ($^{86}Sr/^{87}Sr$ and $^{143}Nd/^{144}Nd$, respectively). Wood specimens from a variety of oak trees and stand locations were pyrolyzed at four temperatures (ranging from 200°C to 800°C) and analyzed using ICP-MS and μ-XRF (X-ray fluorescence) spectroscopy for elemental composition and with multiple collection ICP-MS (MC-ICP-MS) for strontium (Sr) and neodymium (Nd) isotope composition. The concentration of mineral nutrients generally increased with temperature, but the magnitude of the enrichment depended on the element, wood compartment (sapwood vs. heartwood), and geological substrate. The concentrations of rubidium, strontium, manganese, magnesium, potassium, and, to a lesser extent, calcium, were minimally affected by temperature, wood compartment, and substrate. The ratios between the concentrations of these elements, as well as the $^{86}Sr/^{87}Sr$ and $^{143}Nd/^{144}Nd$ isotope ratios, were stable over the entire temperature range. However, only $^{86}Sr/^{87}Sr$ and selected elemental ratios (calcium or magnesium normalized to manganese) were successful for site discrimination. Therefore, our multi-tracer approach provides promising new information to determine the provenance of charred archaeological wood.

Keywords

carbonization – ICP-MS analysis – Itrax Multiscanner – μ-XRF analysis – pyrolysis – wood tracing markers

1 Introduction

Dendrochronology has been used since the 1970s to constrain wood provenance in archaeological studies (Eckstein *et al.* 1975; Hafner *et al.* 2021). Because of its robustness and precision, dendrochronology has become a standard

provenancing method for deciduous oaks and other temperate tree species in Europe (Haneca *et al.* 2009; Fowler & Bridge 2015). However, its application depends on well-established tree-ring chronologies (Towner 2002; Gut 2020), which are not available for all tree species and regions, particularly in the tropics (Edvardsson *et al.* 2021). The requirement of a minimal tree ring number is not met for archaeological charred wood, which is usually found as small fragments (Marguerie & Hunot 2007). The growing demand for provenance studies of archaeological charcoals calls for the development of complementary methods (Jenkins 1989; Fermé *et al.* 2015; Million *et al.* 2018), which can circumvent the drawbacks of studies based on tree-ring width alone (Bridge 2012; Rich *et al.* 2012).

Alternative techniques to trace archaeological woods or commercial timbers are either based on analysis of chronological sequences such as Blue Intensity chronologies (Akhmetzyanov *et al.* 2020a) and wood anatomy (Akhmetzyanov *et al.* 2019; D'Andrea *et al.* 2022), either on bulk proxies such as DNA and haplogroup mapping (Deguilloux *et al.* 2003; Kanno *et al.* 2004; Liepelt *et al.* 2010; Akhmetzyanov *et al.* 2020b), isotopic signatures of carbon (Kagawa & Leavitt 2010), hydrogen (Keppler *et al.* 2007), oxygen (Boner *et al.* 2007; Young *et al.* 2015), and strontium (Rich *et al.* 2016; Hajj *et al.* 2017; Pinta *et al.* 2021), organic markers (Doussot *et al.* 2002; Prida & Puech 2006; Sandak *et al.* 2011; Traoré *et al.* 2018), and multi-elemental composition (Durand *et al.* 1999; Boeschoten *et al.* 2022). These new techniques have proven to be particularly versatile and efficient tools for wood tracing when combined in a multi-proxy approach (Gori *et al.* 2015; Akhmetzyanov *et al.* 2019; Domínguez-Delmás *et al.* 2020).

The multi-elemental and isotopic signatures are better adapted for charred wood provenancing than DNA, stable isotopes (H, C, and O), and organic markers that decompose during thermodegradation. Tracing with elemental and isotopic signatures relies on the similarity between the composition of wood on the one hand and that of underlying soil and rock on the other (DeWalle *et al.* 1991; Marschner 1995). The absorption of nutrients by plant roots is controlled by element bioavailability, which in turn is strongly dependent on soil acidity. In such cases, the concentration ratios of pH-sensitive elements such as Ca, Mg, Mn, and Al might be used as a proxy for soil pH (Kuang *et al.* 2008) and discriminate between sites characterized by different soil acidities.

The isotope ratio of strontium (Sr) $^{87}Sr/^{86}Sr$ is the most relevant tool for sourcing archaeological materials (Bentley 2006; Slovak & Paytan 2012). Strontium is an alkali-earth trace element that is abundant in calcareous rocks, where it substitutes for calcium in the crystal lattice. Isotope ^{87}Sr is a product of the radiogenic decay of ^{87}Rb, which is abundant in silicate rocks, while ^{86}Sr is a stable isotope used as a reference. The $^{87}Sr/^{86}Sr$ ratio of a rock depends

on its initial Sr and Rb contents and the time elapsed since its formation, that is, rock type and age. The power of the "radiogenic" $^{87}Sr/^{86}Sr$ ratio in provenance studies is that, unlike the stable $^{88}Sr/^{86}Sr$ ratio, any isotope fractionation that might occur is cancelled out by correction with a reference value of the $^{88}Sr/^{86}Sr$ ratio. Therefore, $^{87}Sr/^{86}Sr$ ratios reflect only source effects and are not affected by biosynthetic or physiological processes, particularly adsorption and relocation, in plants. Prominent applications of $^{87}Sr/^{86}Sr$ in wood provenance include the identification of the timber wood source in houses in Chaco Canyon, New Mexico, constructed between 850 and 1150 (English *et al.* 2001; Reynolds *et al.* 2005), an antique watercraft from the East Mediterranean (Rich *et al.* 2016), or a 16th-century shipwreck from north-western Spain (Hajj 2017; Domínguez-Delmás *et al.* 2020). Nevertheless, for a given archaeological wood sample, the potential sites of origin might share similar Sr isotope ratios, rendering the disambiguation of wood provenance complicated.

To add constraints for provenance studies in Earth sciences, the Sr isotope ratio is frequently combined with another isotope ratio, the neodymium (Nd) isotope ratio $^{143}Nd/^{144}Nd$. ^{143}Nd is produced by α-decay of samarium-147 (^{147}Sm). Samarium is preferentially incorporated in melts in magmatic processes, leading to its enrichment (and thus higher $^{143}Nd/^{144}Nd$ ratios) in the Earth's mantle over time, compared to the crust (White 2020). Consequently, and similar to the $^{87}Sr/^{86}Sr$ ratio, the $^{143}Nd/^{144}Nd$ ratio varies between rocks of different types and ages and only reflects the source of Nd in biological material. However, unlike Sr, Nd is strongly enriched in silicate minerals compared with carbonate minerals, meaning that soils and thus plants should carry a $^{143}Nd/^{144}Nd$ signature that is reflective mainly of the local underlying silicate component of the rock (e.g., clay minerals in marl layers or limestone). Although Nd isotope ratios are widely applied in Earth Science, for example, to identify the source of detrital sediments (Padoan *et al.* 2011; Bayon *et al.* 2015), only a handful of applications of Nd isotopes exist in archaeological studies, all focusing on glass (Henderson *et al.* 2009; Ganio *et al.* 2012). Here, for the first time, we explore the potential of this marker for historical biological materials.

Altogether, two types of provenance geochemical markers were investigated in this study: (i) elemental ratios and multi-elemental compositions; and (ii) isotope ratios of Sr and Nd, both in bulk wood subjected to carbonization. Although promising, especially for charcoal samples whose number of tree rings is too small to allow dendrochronological provenancing, this combination of markers has never been investigated.

During carbonization, structural organic macromolecules are decomposed, and wood becomes proportionally enriched in mineral nutrients. The elemental composition of wood is expected to vary depending on the degree

of decomposition of individual wood components (e.g., cellulose, hemicellulose, and lignin), as well as on environmental conditions (with or without oxygen). Elements such as calcium, manganese, and magnesium are likely to be less volatile than zinc and sodium (Misra *et al.* 1993). It is generally accepted that carbonization does not have a significant impact on radiogenic isotope ratios in biological materials (Hawley *et al.* 2020; Larsson *et al.* 2020; Ryan *et al.* 2021), in accordance with the fact that such ratios are insensitive to isotope fractionation. For instance, a slight decrease in $^{87}Sr/^{86}Sr$ of charred and uncharred grains reported by Heier *et al.* (2009) was attributed to the variability in biogenic sample composition and contamination. Charring is sometimes even part of sample preparation to remove organic residues prior to digestion (Reynolds *et al.* 2005). The reliability of radiogenic isotopic ratios in determining the source of archaeological material was demonstrated for Sr in calcined bones (Harbeck 2011; Snoeck *et al.* 2015), but to the best of our knowledge, this question was not specifically addressed for wood, let alone for Nd.

Our aim was to verify the preservation of multi-elemental and isotopic signatures during carbonization at different temperatures, and to discuss it with respect to the heterogeneity between wood compartments (i.e., heartwood and sapwood). In addition to bulk concentration measurements using quantitative mass spectrometry (ICP-MS), we explored the potential of semi-quantitative μ-XRF spectroscopy as a complementary, non-destructive, and spatially resolved technique. Although our primary goal was not to address the ability of these markers to prove their provenance, trees from two different sites were selected to check the robustness of the markers with respect to carbonization under different lithological and environmental conditions. This enabled us to introduce the concept of chemical variability of wood between distinct geographical sites and to propose potential relevant markers for future applications in studies on the provenance of carbonized wood.

2 Material and Methods

2.1 *Wood Materials and Sampling Design*

Oak wood from two sites was included in this study: (1) an abandoned coppice woodland, currently undergoing conversion to high forest, growing on a neutral calcisol (pH 6.8) developed on a calcareous substrate composed of limestone, located in Les Cagouillères (Vienne, France: 0.8573° E, 46.6598° N); and (2) a coppice-with-standard growing on an acidic brown soil (pH 3.7) developed on an acidic substrate composed of schists, located in Bogny-sur-Meuse (Ardennes, France: 4.7069° E, 49.8505° N).

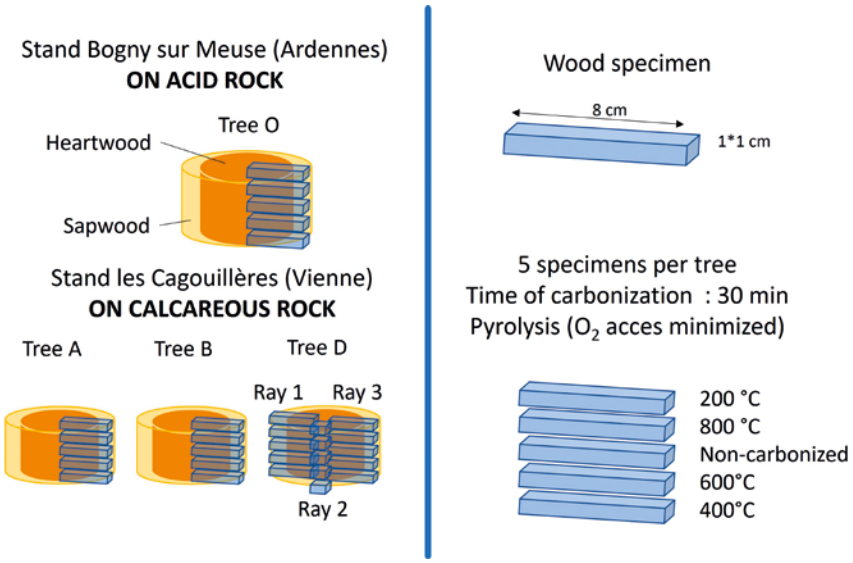

FIGURE 1 Sampling scheme used in this study

Three individuals of *Quercus petraea* (A, B, and D) were selected at the Cagouillères site, and one individual of the same genus (tree O) was selected at the Bogny-sur-Meuse site. All trees were selected among individuals with similar dendrological characteristics, with heights between 17.7–20.3 m, and a diameter between 20.75–33 cm, and free of any physical or sanitary damage. Trees A, B, and D were 62 years old, and tree O was 68 years old (Dufraisse *et al.* 2018). A section of the trunk taken at a height of 7 m was sectioned into disks, from which a sample series of five parallelepipedal specimens of approximately $1 \times 1 \times 8$ cm were cut out. Three sets of specimen series were taken from a single tree, D, from the Cagouillères site to evaluate intra-individual variation. Although these pseudo-replicates cannot be considered strictly independent samples, they provide the first estimation of the expected intra-tree variability. Thirty wood specimens were prepared from four trees following the sampling scheme presented in Fig. 1. The samples were air-dried and stored in polypropylene bags prior to carbonization.

2.2 *Carbonization*

Wood specimens enclosed in aluminium foil to prevent access to oxygen were heated for 30 min. in a muffle furnace at 200°C, 400°C, 600°C, or 800°C. A control sample was placed in each tree. The heartwood/sapwood boundary was identified on non-carbonized specimens by observing the wood colour and tylosis distribution under an optical microscope, following the protocol

of Dufraisse *et al.* (2018). The number of heartwood tree rings counted on the non-carbonized specimens was then used to locate the boundary between the hardwood and sapwood in the corresponding carbonized specimens.

2.3 *Multi-Elemental and Isotopic Analysis*

The multi-elemental composition of the wood specimens was determined using two independent techniques: *in-situ* μ-XRF (X-ray fluorescence) spectroscopy, which produces scans of signal intensity converted to relative concentrations in arbitrary units (a.u.), and inductively coupled plasma mass spectrometry (ICP-MS), yielding absolute concentrations in parts per million (ppm) for bulk samples. Relative concentrations from μ-XRF spectroscopy were kept in the form of arbitrary units, as the lack of equivalent reference material, that is, burnt and of biological origin, prevented any calibration of absolute concentration. Bulk ICP-MS measurements were systematically performed as part of the protocol for isotope-ratio measurements. Being a precise yet time-consuming method, ICP-MS analyses were carried out only on 12 specimens representing various descriptive factors of the sample set (carbonization temperature, site, tree, and heartwood/sapwood, Table 1). μ-XRF scans were acquired for all wood specimens (n = 30).

TABLE 1 Summary of elemental analyses of wood specimens performed in this study

Temperature	**Non-carbonized**	**200°C**	**400°C**	**600°C**	**800°C**
Tree A	Sapwood*	Sapwood	Sapwood	Sapwood	Sapwood
	Heartwood*	Heartwood	Heartwood	Heartwood	Heartwood
Tree B	Sapwood*	Sapwood	Sapwood	Sapwood	Sapwood
	Heartwood*	Heartwood	Heartwood	Heartwood	Heartwood
Tree D (ray 1)	Sapwood*	Sapwood	Sapwood*	Sapwood	Sapwood*
	Heartwood*	Heartwood*	Heartwood*	Heartwood*	Heartwood*
Tree D (ray 2)	Sapwood	Sapwood	Sapwood	Sapwood	Sapwood
	Heartwood	Heartwood	Heartwood	Heartwood	Heartwood
Tree D (ray 3)	Sapwood	Sapwood	Sapwood	Sapwood	Sapwood
	Heartwood	Heartwood	Heartwood	Heartwood	Heartwood
Tree O	Sapwood*	Sapwood	Sapwood*	Sapwood	Sapwood*
	Heartwood*	Heartwood*	Heartwood*	Heartwood*	Heartwood*

* Analysed by both μ-XRF spectroscopy and ICP-MS, the rest were analysed only by μ-XRF spectroscopy.

2.3.1 *In-Situ* μ-XRF Spectroscopy and Microdensitometry

Coupled, spatially resolved measurements of multi-elemental distribution and radiographic density were performed using an Itrax Multiscanner (Cox Analytical Systems, Mölndal, Sweden) equipped with a μ-XRF detector and an X-ray photodetector. The X-ray source was a Cu target tube operated at a voltage of 50 kV and a current of 30 mA using a scanning step of 500 μm. The X-ray beams used for microdensitometry and μ-XRF spectroscopy were 10 μm and 100 μm in size, respectively. The peaks of Al, P, Ni, Fe, S, K, Cr, Ca, Mn, Ti, and Cl were identified in the μ-XRF spectra by semi-automatic detection with the Qspec software. Compared to elements detected by bulk elemental analysis with ICP-MS (Section 2.3.2), the list was short of Sr, Rb, and Nd, all present below the μ-XRF detection limit, and of Mg and Cu, whose peaks interfered with those of the Cu target tube.

2.3.2 Bulk Chemical and Isotope Composition

The specimens were split into heartwood and sapwood, each ground separately in a cutting mill with a 2 mm sieve. Three aliquots of approximately 500 mg of sawdust from each sample were weighted to the nearest 0.1 mg with an analytical balance in 15 ml disposable glass vials. The number of aliquots was adjusted for samples with low amounts of material (carbonized sapwood). Each glass vial was washed with hot, ultrapure nitric, and hydrochloric acids, rinsed with ultrapure water (> 18.2 MOhm), and dried overnight. Each sample was suspended in 5 ml of 69% nitric acid (Optima grade, Fischer Chemical) and digested in batches of 15 using a microwave-assisted system (Milestone Ultrawave) at 220°C and 110 bar for 40 min. Digested samples were centrifuged, and the supernatant was collected and diluted with ultrapure water to a TDS (total dissolved solids) of 0.25% and an acid percentage of 6%. In each batch, at least two blanks and one reference material (SRM INCT OBTL5, tobacco leaves) were included in the wood sample. The elemental concentrations were quantified by ICP-MS (Thermo iCap TQ, Thermo Fisher, Bremen, Germany) as follows: The instrument was tuned for oxide and doubly charged ions. The single quadrupole—Kinetic Energy Discrimination (SQ-KED) mode and TQ-O2 (Triple Quadripole Oxygen) reaction and mass-shift modes were used to limit or eliminate potential interference. External calibration was performed using synthetic multi-elemental solutions (TECHLAB) acidified with 2% HNO_3 (v/v). The accuracy of the calibration was checked with certified reference surface water (SPS-SW1), and the instrumental drift was monitored by running SPS-SW1 every 10–20 samples and by adding Rh and Ir to the

samples as internal standards. The measurements were performed three times and averaged for each solution. The reference material INCT OBTL5 (tobacco leaves) was used to check the accuracy of the method, and procedural blanks were measured to assess contamination (Table A1 in the Appendix).

Strontium and neodymium were separated from the sample matrix in the digestion solution by extraction chromatography based on specific resins: Sr-SPEC resin (50–100 μm size; Eichrom) for Sr (Hajj 2017) and TRU-SPEC and Ln-SPEC resins for Nd (Eichrom) (Caro *et al.* 2006; Cogez *et al.* 2015) at the High-Resolution Platform (PARI) of the Institut de Physique du Globe de Paris (IPGP). Columns loaded with 0.2 ml of the Sr-SPEC resin were washed with Milli-Q water and ultrapure acids (5 M HNO_3 and 6 M HCl) prior to sample introduction, while matrix elements and Sr were eluted with HNO_3 3 M and Milli-Q water, respectively. Neodymium was extracted in a two-step separation: first, on columns loaded with 0.5 ml TRU-SPEC resin washed with ultra-pure HNO_3 2 N and Milli-Q water, where rare earth elements were eluted with Milli-Q water, and then on a column loaded with 2 ml of Ln-SPEC resin, previously washed with Milli-Q water and ultra-pure HNO_3 6 N, and where Nd was selectively eluted with 0.25 M HCl. Isotope ratios $^{87}Sr/^{86}Sr$ and $^{144}Nd/^{143}Nd$ were acquired during separate measurement sessions using a Multi-Collector Inductively Coupled Plasma Mass Spectrometer (MC-ICP-MS; Neptune Plus ThermoFisher Scientific) in low-resolution mode at the PARI platform of the IPGP. Solutions were introduced into the mass spectrometer using an APEX desolvation unit (for Sr solutions) and a cyclonic spray chamber (for Nd solutions) connected to a PFA nebulizer (50–100 μl/min, depending on the measurement session). The Sr and Nd concentrations in the loading solutions were approximately 100 ppb and 5 ppb, respectively. Because of the low concentration of Nd in some of the wood samples (a few ppb of dry mass), it was sometimes difficult to obtain sufficient amounts of Nd for isotope analyses. Therefore, the corresponding data were discarded because of deteriorated precision and accuracy at these signal levels, as indicated by the measurement of standard solutions of known isotope compositions at similar levels. To reduce the formation of oxides, N_2 was used as an additional gas during Nd measurement sessions. Ions were detected using Faraday cups, with masses of 86 and 146 in the centre cup for Sr and Nd, respectively. Blank signals were corrected using on-peak zeroes (leading as well to the subtraction of Kr-86 for Sr measurements), and mass-dependent isotope fractionation was corrected by using the "natural" ratios $^{88}Sr/^{86}Sr$ (8.3752) and $^{146}Nd/^{144}Nd$ (0.7219). For samples measured three times, the average ratio and 95% confidence interval according to the Student's t-distribution were calculated. For samples measured fewer than three times, the 95% confidence interval was estimated from the

two standard errors of the repeated measurements of the reference material (processed through powder digestion and separation as wood samples). The reference materials NIST-987 and NIST-3135a were checked for the accuracy of Sr and Nd isotope ratio measurements and procedural blanks for contamination rates (Table A1 in the Appendix). Equation (1) was used to express Nd isotope ratios on the relative εNd scale by normalizing $^{143}Nd/^{144}Nd$ ratios to the $^{143}Nd/^{144}Nd$ ratio of the "chondritic uniform reservoir" (CHUR = 0.512638).

$$\varepsilon\mathrm{Nd} = \left[\frac{\left(\frac{^{143}\mathrm{Nd}}{^{144}\mathrm{Nd}} \right)_{\mathrm{sample}}}{\left(\frac{^{143}\mathrm{Nd}}{^{144}\mathrm{Nd}} \right)_{\mathrm{CHUR}}} - 1 \right] \cdot 10^{4} \quad (1)$$

2.4 *Data Analysis*

2.4.1 Mass, Volume, and Density Measurements

The specimens were weighed systematically before (m_{before}) and after (m_{after}) carbonization, and the relative mass loss (RML) was computed as the difference in the weight of the identical specimen before and after carbonization.

$$RML = \frac{m_{after} - m_{before}}{m_{before}} \cdot 100 \quad (2)$$

The specimen size (transverse surface and longitudinal thickness) and density of the specimens were assessed after carbonization, and their relative loss (RL) was computed by comparing the values between the control and carbonized specimens.

$$RL(x) = \frac{x_{carbonized} - x_{control}}{x_{control}} \cdot 100 \quad (3)$$

Wood density was assessed in two independent ways. First, the bulk specimen density was determined as the ratio of mass to volume of the total specimen, where the volume was estimated from the dimensions measured after carbonization. Second, *in-situ* radiographic density was determined based on the X-ray intensity detected by the Itrax Multiscanner. The significant correlation (r = 0.99, n = 30) between these two estimates lends confidence to the radiographic density estimates.

2.4.2 Elemental Composition of Wood

Micro-XRF spectroscopy has a number of advantages relevant to archaeological and heritage samples, such as a short acquisition time, little sample preparation, and non-destructive analysis, but it is not able to detect elements in trace amounts and has lower accuracy compared to ICP-MS. Except for intra-tree variation study, we relied on ICP-MS data. The comparison between the two techniques provided in Section A1.2 in the Appendix demonstrated that the concentration data from μ-XRF spectroscopy were correlated with those from ICP-MS ($r > 0.75$) for P, Ca, K, and Mn. The two methods were less strongly correlated at high temperatures; therefore, any comparison between different degrees of carbonization based on μ-XRF spectroscopy data should be made cautiously. For the purpose of this study, we focused on the bulk chemical composition of wood rather than on the chronology of tree development and the μ-XRF scans were treated as average concentrations over wood compartments and specimens.

Before data processing, individual measurements were checked for outliers, which were identified as values differing by a factor of 10 or more from the average concentration value. Outliers were removed for two wood specimens measured with ICP-MS measurements (two measurements from the tree's D heartwood at 600°C and one measurement from the tree's D ray 2 sapwood carbonized at 800°C) and one measurement from μ-XRF scan (from the tree's D ray 1 non-carbonized). Elemental and isotope composition data were further processed using R software (version 4.1.2).

Descriptive analysis was carried out with principal component analysis (PCA) on a dataset of ICP-MS concentrations ($n = 58$) with carbonization temperature as a supplementary quantitative variable and wood compartment and site as supplementary qualitative variables, with the help of the "fviz_pca" function from the package "factoextra" (Kassambara & Mundt 2020).

Linear models were selected with the help of the AIC score computed by the function AIC (Table A1 in the Appendix) and processed with ANOVA type 2. Models were checked for the normality of their residual distributions by plotting histograms and quantile-quantile plots. The significance of random effects was evaluated with the help of a Chi-Square test using the function "ranova" from the package "ImerTest" (Kuznetsova *et al.* 2017).

First, a model for non-carbonized wood was constructed using the average relative elemental concentrations from μ-XRF spectroscopy ($n = 10$) as a response variable and wood compartment (heartwood/sapwood), tree, and ray as explanatory variables. The wood compartment was considered a fixed effect because of its fixed relationship with chemical composition, while

concentrations in trees and rays, which vary depending on individual observations, were treated as random effects. Two sub-models were constructed: one with relative concentrations in the form of arbitrary units and the second with relative concentrations normalized to wood density to reduce the matrix effects. In XRF, density is linked to signal intensity, and μ-XRF fluorescence is more strongly absorbed by high-density samples. To study intra-tree variation, a simplified model including only the wood compartment as a fixed effect and the ray as a random effect was applied to a subset of non-carbonized specimens of the three rays of tree D. The adjusted variation associated with the ray effect was computed with the help of the "icc" function from the package "performance" (Lüdecke *et al.* 2021). We noted that the dataset was unbalanced regarding the site factor, with only one tree from the Bogny-sur-Meuse location and three trees from the Cagouillères location.

The second model was based on the ICP-MS concentrations (n = 58) in response to the effects of temperature, wood compartment, their interaction, and trees. Consistent with the previous model, the tree was considered a random effect, whereas temperature and wood compartments were fixed effects. The concentrations were first normalized to the corresponding Rb concentrations (from the same wood compartment and tree), as Rb was identified as the most thermostable element (Section 3.3). The last model was constructed to modelize the μ-XRF relative concentrations as a function of ICP-MS concentrations in interaction with the heartwood/sapwood factor and carbonization temperature, all considered as fixed effects.

2.4.3 Elemental Mass Loss

To determine the change in elemental composition during carbonization, independent of total mass loss, the elemental mass loss (ML_{el}) was computed as the change in the mass of element (m_{el}) between non-carbonized specimen and specimen carbonized at 800°C (Equation (4)). The mass of the element (m_{el}) was calculated as a product of the ICP-MS concentration and the total mass of the specimen.

$$ML_{el} = \frac{m_{el800°C} - m_{el\_control}}{m_{el\_control}} \cdot 100 \quad (4)$$

In this context, an ML_{el} value of 0% meant no elemental mass loss, whereas a value of –50% indicated that half of the element mass was lost during carbonization. Elements with an ML_{el} close to zero were considered the most refractory (i.e., the least volatile).

3 Results

Data used for analyses in the article are available at https://doi.org/10.1163/27723194-bja10019.

3.1 *Elemental Composition of Non-carbonized Wood*

The highest concentrations in wood were reached by K, Ca, S, Mg, Al, and P (Fig. 2 with the bulk heartwood of trees from the calcareous site), with a decrease in concentration in the aforementioned order from 10^6 ppb for K to 10^4 ppb for P. The concentrations of other elements (Fe, Mn, Rb, Cu, Sr, Zn, Ni, Cr, and Nd) ranged from 10^4 ppb for Fe to less than 10 ppb for Nd. The bulk elemental composition of sapwood was similar to that of heartwood, albeit with higher concentrations of some of the most abundant elements. The tree from the acidic site had a composition similar to that of the trees from the calcareous site (Fig. A1 in the Appendix), except for Mg and Ca (twice more abundant

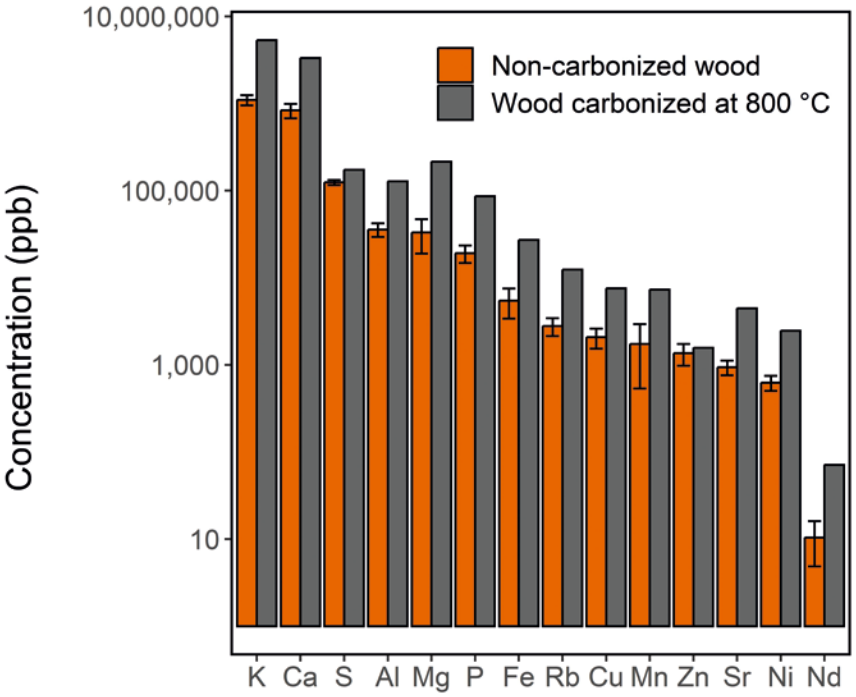

FIGURE 2 Concentration of mineral nutrients in the heartwood of the trees A, B and D from the calcareous site Cagouillères, with log-scale for the *y*-axis. Brown bars indicate non-carbonized wood (average, $n = 3$, SD), and gray bars wood carbonized at 800°C. Elements are sorted along the *x*-axis by decreasing values of concentration in non-carbonized wood.

at the calcareous site) and Mn (five times more abundant at the acidic site). The major mineral nutrients in wood, K and Ca, together accounted for at least 80% of the mineral content measured in our tree samples. Additionally, Mg, S, P, Al, and Mn occurred at lower but still relevant amounts, between 0.5 and 5% of the total measured mineral content.

The variability in relative concentrations measured by μ-XRF-spectroscopy within non-carbonized wood was assessed for trees A, B, and D, the latter with rays 1, 2, and 3, all of which were grown at the calcareous site. Using the model based only on relative concentrations (Model 1 in Table 2), Fe and Mn tended to vary the most, and their differences were statistically significant with respect to the three effects: wood compartment, tree, and ray. In addition, Cr, Ni, and Ca varied significantly between wood compartments, and Cr and Ca varied significantly between trees and rays. In the model based on relative concentrations weighted by density (Model 1 in Table 2), Fe, Mn, and P varied significantly between wood compartments, whereas only Mn revealed significant differences depending on tree and ray. Normalization by density contributed to diminishing the inter- and intra-tree variability of trace elements (Ni and Cr), meaning that such normalization might be useful for detecting

TABLE 2 Results of ANOVA for a model based on average relative μ-XRF elemental concentrations of non-carbonized wood from Cagouillères (trees A, B and D, and rays 1, 2 and 3, $n = 10$) as a function of wood compartment, tree and ray

Element	Wood compartment		Tree		Ray	
	Model 1	Model 2	M1	M2	M1	M2
Fe	43.14***	16.58***	***		***	
Ni	39.06***					
Cr	33.4***		***		***	
Mn	16.94***	10.12***	***	***	***	***
Ca	9.33***		*		*	
P		5.94*				
K						
S						
Al						

Model 1 (M1) was computed using arbitrary units of μ-XRF data and Model 2 (M2) was computed using μ-XRF data normalized to radiographic density. *** $p < 0.001$, ** $p = 0.001$–0.01, * $p = 0.01$–0.05, otherwise blank. *F*-values presented for $p < 0.05$. Elements are sorted by decreasing values of *F*-value for wood compartment effect.

variations in elements with limited quantification accuracy with μ-XRF spectroscopy (Section A1.2 in the Appendix). The higher concentrations of mineral nutrients in sapwood were also inferred from ICP-MS measurements (Fig. A2 in the Appendix). The strongest enrichment of sapwood over heartwood was recorded for P (987 ± 52%, n = 3, SD, ICP-measurements), Mg (915 ± 61%), and Mn (743 ± 34), and a minor enrichment was noted for S, K, Rb, and Ca; for transition elements such as Fe, Ni, and Cu, the increase was negligible.

The bulk ICP-MS analyses of heartwood and sapwood were compared to the elemental distribution along the radial axis (i.e., from the pith to the bark) using μ-XRF. In general, concentrations of mineral nutrients were higher in the outermost rings than close to the pith, and the correlation coefficient between concentration and distance from the pith was between −0.25 and 0.60, with all elements correlating significantly and positively, except for Ni and Cr, which correlated significantly and negatively. In comparison, the correlation between density and concentrations, and between radiographic density and distance from the pith were both significant, but weaker, with a correlation coefficient within 0.01–0.40 for the former, and around 0.21 for the latter. For Mn and to some extent for K, the concentrations within the sapwood and heartwood compartments were nearly constant, although they indicated an abrupt change at the sapwood/heartwood boundary (Fig. A3 in the Appendix).

The average elemental composition was significantly different from one ray to another (p-value of Chi-Square test < 0.005). In the mixed model combining the ray effect and the wood compartment effect, the former was not strong except for Cr (49.01% of variation due to ray effect) and to some extent for Ni (21.66% of variation due to ray effect against 8.74% of variation due to wood compartment effect; Table 3). The compartment effect on Ca and Mn concentrations was stronger than that of the ray effect, in line with the important wood compartment effect inferred above.

TABLE 3 Relative adjusted variation of random effect of ray and of fixed effect of wood compartment in % compared to the total variation (with ray and wood compartment induced variation and residual variation)

Element	**Cr**	**Fe**	**K**	**Ni**	**S**	**P**	**Ca**	**Mn**	**Al**	**Ti**
Ray variation (%)	49.01	25.08	24.98	21.66	20.27	19.17	16.31	9.87	2.15	0.13
Compartment variation (%)	19.98	21.46	23.41	8.74	36.12	11.21	34.53	45.70	1.07	12.70

Elements are sorted by decreasing values of ray variation (n = 6).

3.2 *Effect of Carbonization on Wood Density*

Average density calculated for specimens carbonized at the same temperature (n = 6) ranged from 787.1 ± 37.9 g/dm³ for non-carbonized wood to 434.1 ± 49.2 g/dm³ for wood carbonized at 800°C. Carbonization at 800°C led to an average mass loss of 81.3 ± 1.0% and to a decrease of 47.2 ± 5.3% and of 44.3% ± 5.8% in terms of density and average radiographic density, respectively (Fig. 3). The mass and density did not decrease at a constant rate throughout carbonization, with wood undergoing a major change between 200 and 400°C, which accounted for 79 ± 17% of the overall density decrease and 66 ± 12% of the total mass loss. The strong mass loss between 200 and 400°C split the population of wood specimens into two clusters: the low-temperature and high-density samples (non-carbonized and carbonized at 200°C) and high-temperature and low-density samples (carbonization temperatures of 400, 600, and 800°C). Within the two groups, changes were inferior to 10% between successive carbonization steps. In the high temperature group, the density decrease was particularly low between 600 and 800°C. In this step, trees A and D displayed an

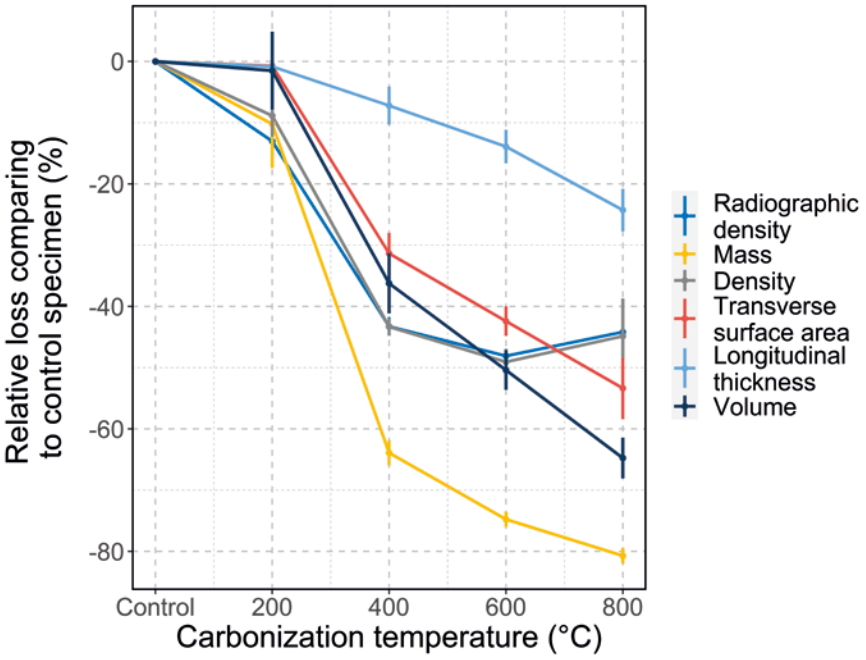

FIGURE 3 Average over specimens of trees A, B, D and O (n = 6, SD is depicted as error bars) relative loss of mass, density (quantified in two different ways: bulk density and from radiographic density measurements averaged over the entire specimen), and dimensions (transverse surface area, longitudinal thickness, and volume) between each carbonization steps

inverse trend (i.e., the density increased instead of decreasing). Mass loss was significantly (p-value < 0.05) and strongly (r = 0.95) correlated with temperature, responsible for 38% of the mass loss.

3.3 *Changes in Wood Elemental Composition during Carbonization*

Temperature was positively correlated with the concentrations of all analysed elements, particularly Sr, Nd, and Ni (Fig. 4a and Fig. A1 in the Appendix). At 800°C, the concentrations were between 10^6 ppb (K and Ca in sapwood from the calcareous site) and 10 ppb (Nd in heartwood from the calcareous site) and increased by a factor of 0.95 (Zn) to 4.8 (Rb) relative to non-carbonized wood. In comparison, at the same temperature, specimens lost, on average, 63% of their volume and 48% of their density. K and Ca remained the most abundant elements in carbonized wood, and their relative contributions to the overall mineral content even increased, reaching 92.9% in wood carbonized at 800°C. The temperature was strongly correlated with the first PCA axis, explaining 51.5% of the variation, which indicated its dominant impact on the overall dataset variability (Fig. 4c). The second axis singled out elements S, Ca, and Mg associated with sapwood and calcareous sites, and elements Al, Fe, and Nd associated with heartwood and acidic sites. Sapwood and heartwood were clearly distinguished on the second axis and partially on the first axis (Fig. 4d). The sites overlapped on the first axis but were discriminated on the second axis (Fig. 4b). Nevertheless, the localization of several samples into non-corresponding site groups (Fig. 4b) indicated a slight interference between heartwood/sapwood and site factors. The interaction between the site and the wood compartment was not tested because of the small number of samples per site (Section 2.4.2).

PCA indicated that elemental concentrations in carbonized wood were influenced by multiple factors, and it would be impossible to firmly associate a single concentration value with a specific substrate without further information on other factors, especially the carbonization temperature. Such information is rarely available for archaeological samples, and for charred wood provenancing, it is necessary to define how to constrain the effect of temperature. Although the elemental concentrations and the density of carbonized wood were generally negatively correlated, the corresponding correlation coefficient ranging from −0.24 to −0.55 (excluding Cr) implied that the strength of this correlation was highly element-dependent. To identify elements that increase their abundance proportionally to the total mass loss, the elemental mass loss ML_{el} was computed according to Equation (4) in Section 2.4.3. Rubidium (Rb) was identified as the most refractory element during our

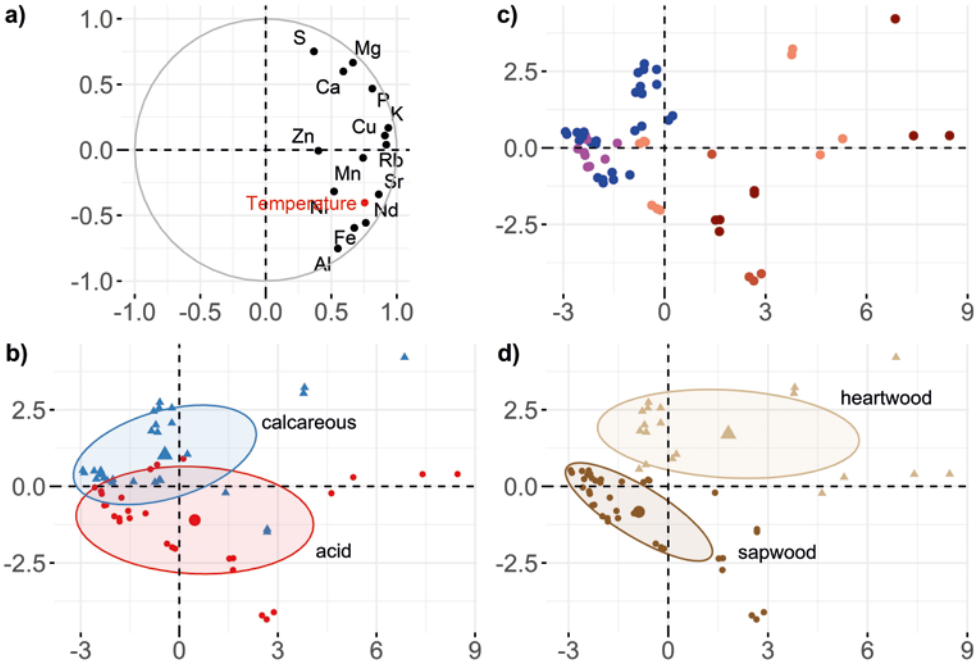

FIGURE 4 Result of PCA of ICP-MS concentration data (n = 58) for axes 1 and 2, representing 51.5 and 22% of dataset variation, respectively. (a) Diagram of variables, with supplementary variable temperature in red. (b, c, d) Diagrams of individuals, with large points representing centers of gravity of point clouds. (b) Individuals are distinguished between the acidic site in red and the calcareous site in blue. (c) Individuals are distinguished using a color gradient going from dark blue for non-carbonized individuals to dark red for individuals carbonized at 800°C. (d) Individuals are distinguished between heartwood in light brown and individuals from sapwood in dark brown.

carbonization experiments (i.e., the element whose absolute amount in wood remained almost constant during carbonization) with ML_{Rb} of −9.77 ± 3.67%, implying that only approximately 10% of Rb mass was lost during carbonization at 800°C (Fig. 5).

Elements K, Mg, Nd, Sr, and Mn had ML_{el} values between −10 and −30% and could be considered as rather refractory elements for the purpose of our study. On the contrary, S and Zn underwent losses of almost 80%. It is worth noting that ML_{Zn} (−82.07 ± 1.58%) was close to the total mass loss of 81.3 ± 1.0% implying that Zn likely volatilized at the same rate as major wood components, such as cellulose and hemicellulose, which are composed only of H, C, and O. The behaviour of Ca during carbonization was ambiguous, as it appeared rather refractory for wood from the calcareous site but was subjected to a relative loss

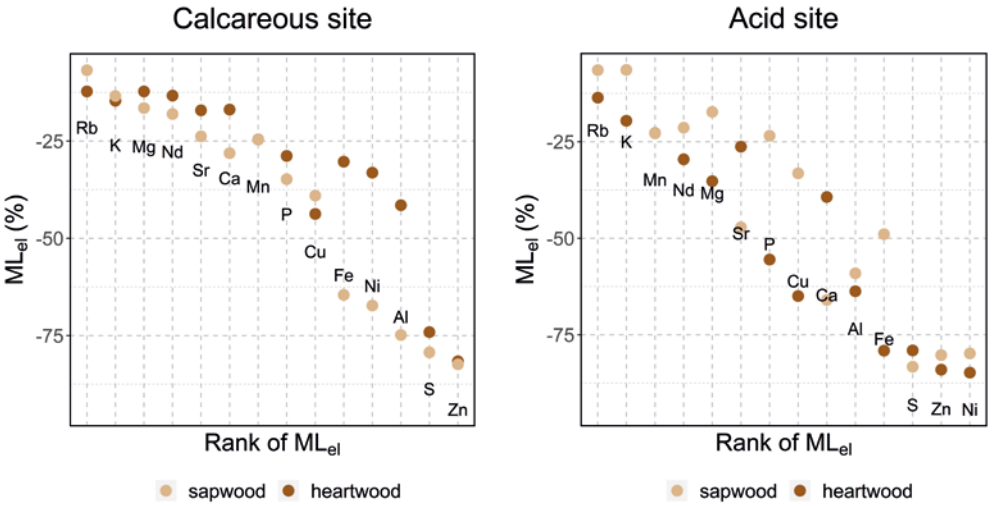

FIGURE 5 Elemental mass loss ML_{el} in wood carbonized at 800°C compared to non-carbonized wood. Heartwood is depicted in dark brown and sapwood in light brown from calcareous (left panel) and acidic (right panel) sites. Elements are sorted along the X-axis by decreasing values of average ML_{el} for heartwood and sapwood.

of 40–65% for wood from the acidic site, where ML_{el} tended to be higher for all elements and particularly for Fe, Al, and Ni. Additionally, ML_{Ca} was considerably different between sapwood (66.0%) and heartwood (39.3%), whereas for refractory elements, this difference was less than 10%. Values of ML_{el} for a given element were not consistent between the heartwood and sapwood of the two sites, suggesting a differential effect of carbonization within each wood compartment.

The impact of temperature on concentrations was examined through a model that included the effects of wood compartments and trees (Table 4). The difference in the effect of carbonization on heartwood and sapwood hypothesized above was not confirmed, as the interaction between temperature and the wood compartment was found to be insignificant. To evaluate the thermostability of the elements, their individual concentrations were normalized to the corresponding Rb concentration. The effect of temperature (p-value < 0.05) on the elements P, K, Mg, Ca, Nd, Sr, and Mn was not significant when expressed as a relative concentration with Rb. The model ascertained the poor thermostability of Al, S, Cu, and Ni (Fig. A2 in the Appendix). The difference between wood compartments was significant for Al, Nd, Mg, Cu, and Ca, in addition to Mn and P, for which a difference between compartments was already observed in non-carbonized wood (Table 2). The tree effect represented both the site and the individual, and its significance for Mn, Ca, Sr, Cu, and P was possibly derived from the difference between the two sites.

TABLE 4 Results of ANOVA for a model based on ICP-MS concentrations normalized to Rb concentrations (trees A, B, D and O, $n = 20$)

Element/Rb	Temperature	Wood compartment	Tree
P		131.29***	*
Al	11.65***	45.81***	
Mn		32.34***	***
Nd		31.47***	
Mg		29.84***	
Cu	14.86***	14.79***	***
Ca		12.11***	***
Sr			***
Ni	4.86*		
Fe			
Zn			
K			***
S	36.41***		

*** $p < 0.001$, ** $p = 0.001$–0.01, * $p = 0.01$–0.05, otherwise blank. *F*-values presented for $p < 0.05$. Elements are sorted by decreasing values of *F*-value for wood compartment effect.

3.4 *Sr Isotope Signatures*

The $^{87}Sr/^{86}Sr$ ratios of non-carbonized wood from trees at the calcareous site varied between 0.71265 (tree A sapwood) and 0.71486 (tree B sapwood), with a global mean ± SD value of 0.71368 ± 0.00075 ($n = 6$) and 0.71381 ± 0.00103 ($n = 3$) for heartwood and 0.71356 ± 0.00115 ($n = 3$) for sapwood (Fig. 6). Tree O grown on acidic site had a global $^{87}Sr/^{86}Sr$ ratio of 0.71736 ± 0.00026, with 0.71741 in heartwood and 0.71714 in sapwood. The difference between the $^{87}Sr/^{86}Sr$ ratios of the non-carbonized sapwood and non-carbonized heartwood was 0.00032 ± 0.00029 (average calculated from heartwood/sapwood differences per tree, $n = 4$). For trees D and O measured at all temperatures, the $^{87}Sr/^{86}Sr$ ratios of carbonized and non-carbonized wood ranged from 0.71288 to 0.71377 for tree D (calcareous site) and 0.71709–0.71779 for tree O (acidic site). According to the linear model including temperature, wood compartment, and trees (Table 5), both wood compartment (*F*-value = 12.79, *p*-value = 0.003) and temperature (*F*-value = 7.17, *p*-value = 0.018) had significant impacts on the Sr isotope ratio. Heartwood had higher $^{87}Sr/^{86}Sr$ ratios than sapwood, and $^{87}Sr/^{86}Sr$ ratios tended to slightly decrease with temperature, with a visible step between 200 and 400°C. Nevertheless, it was the variation induced by trees, including

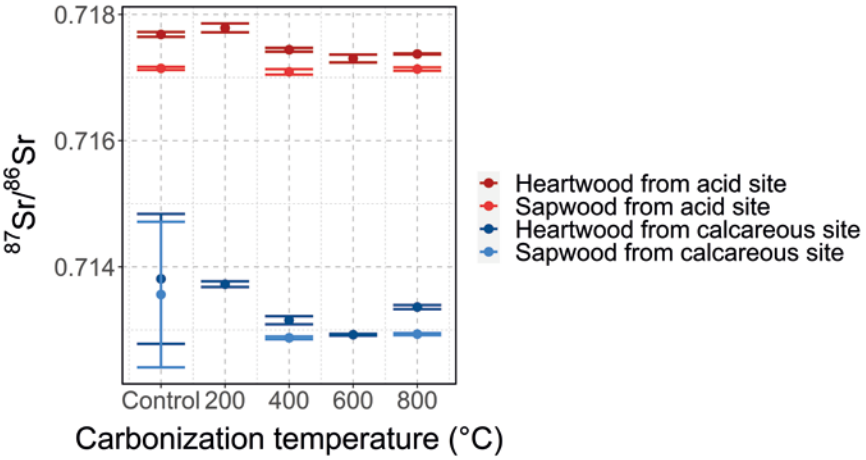

FIGURE 6 Average $^{87}Sr/^{86}Sr$ ratios over wood specimens from the trees A, B and D (n = 3, 95% CI) from the calcareous site (blue labels) and from the tree O from the acidic site (red labels) carbonized at different temperatures. Dark shades indicate heartwood, light shades sapwood.

differences in their geographical origin that was responsible for 96% of the Sr isotope variation over the whole dataset, and both wood compartment and temperature effects were thus regarded as very weak.

3.5 *Nd Isotope Signatures*

εNd of non-carbonized wood from trees at the calcareous site varied between −9.3 (tree A sapwood) and −11.6 (tree B heartwood), with a global mean ± SD value of −10.4 ± 1.0 (n = 6), and −11.3 ± 0.5 (n = 3) for heartwood and −9.6 ± 0.4 (n = 3) for sapwood (Fig. 7). The εNd dataset did not comply with the requirement of a minimal number of measurements to perform the model previously used for elemental and Sr isotope data (Section 2.5), such that only partial ANOVA tests were performed. The ANOVA test (p-value < 0.05, not shown here) indicated the absence of any significant difference between trees at the same site (calculated for non-carbonized wood from trees A, B, and D from the calcareous site, n = 6). The relationship between εNd values in heartwood and sapwood was unclear: for non-carbonized wood, the εNd values of heartwood and sapwood of tree D overlapped with uncertainty, although heartwood was characterized by a somewhat lower εNd value, whereas at 800°C, sapwood displayed lower εNd values than heartwood (Fig. 7). The values of εNd for non-carbonized sapwood of trees A, B, and D from the calcareous site lay within the same range as those of tree O from the acidic site, such that the two

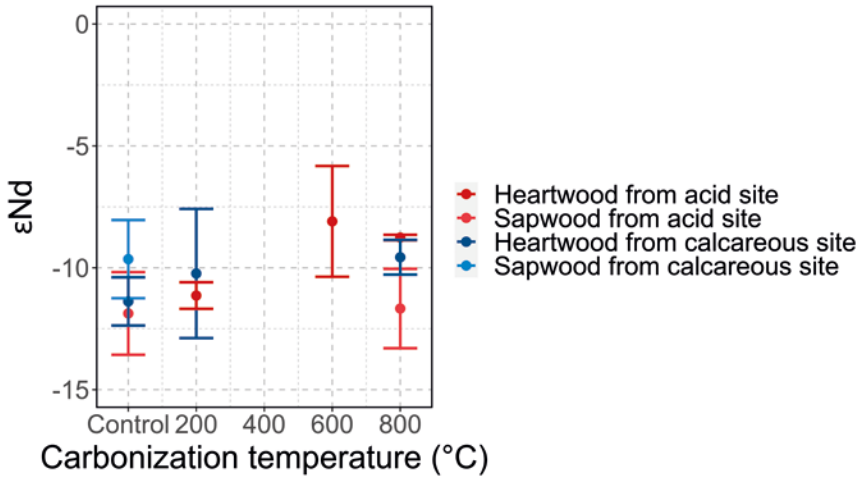

FIGURE 7 Average εNd over wood specimens from the trees A, B and D (n = 3, 95% CI) from the calcareous site (blue labels) and from the tree O from the acidic site (red labels) carbonized at different temperatures. Dark shades indicate heartwood, light shades sapwood.

sites were not distinguishable in terms of their wood Nd isotopic signatures. However, the similarity in εNd values for the tree O sapwood (acidic site) and for the tree D heartwood (calcareous site) between 0 and 800°C supported the negligible role of carbonization.

4 Discussion

4.1 *Effect of Carbonization on Geochemical Markers of Carbonized Wood*

Elements defined as refractory in Section 3.3 complied with the first requirement of charred wood provenancing, which was a constant signature throughout carbonization. Nevertheless, we were unable to test the second requirement of site separation in this study because of the small number of sampling sites and individuals. Therefore, the effect of carbonization was tested on the Ca/Mn, Ca/Al, Mg/Mn, and Ca/Al ratios, which have been reported as sensitive to soil pH changes in previous studies (Kuang *et al.* 2008; Chen *et al.* 2010; Kwak *et al.* 2011). Throughout our experiments, these elemental ratios did not change depending on temperature, but on wood compartment except for Mg/Mn (Table 5). In contrast, Mg/Mn had the highest sensitivity to tree

TABLE 5 Results of ANOVA over selected geochemical markers as a function of temperature, wood compartment and tree

Element	Temperature	Wood compartment	Tree
Mn/Al		18.72***	*
Ca/Al		13.88***	*
Ca/Mn		6.19*	*
Mg/Mn			***
$^{87}Sr/^{86}Sr$	7.17*	12.79***	***

*** $p < 0.001$, ** $p = 0.001–0.01$, * $p = 0.01–0.05$, otherwise blank. *F*-values presented for $p < 0.05$. Elements are sorted by decreasing values of *F*-value for wood compartment effect.

effect. As depicted in Fig. 8, the Ca/Mn and Mg/Mn ratios revealed similar offset between the calcareous and acidic sites (factor 100). The Ca/Al and Mn/Al ratios were ca. 10 times higher for the calcareous site than for the acidic site, but the sapwood ratios from one site overlapped with the heartwood ratios from the other site.

In addition to these markers, which were previously reported to be characteristic of the wood site of origin, we explored the potential of other elemental ratios capable of discriminating wood provenance based on the results of the linear discriminant analysis performed on the ICP-MS data (Table 6). Among the contributors with an absolute value of loading > 0.5, the selection was restricted to the refractory elements Ca, Nd, Mn, Fe, and Sr. With the help of PCA (Fig. 4), Ca was identified as a characteristic of the calcareous site, while other elements were associated with the acidic site. In particular, the concentrations of Ca normalized to Sr and Nd were approximately 10 times higher for the calcareous site than for the acidic site. Amongst the thermostable elemental ratios, the Ca/Mn and Mg/Mn ratios showed the highest discrimination potential for carbonized wood, given the high inter-site and low wood compartment differences in our dataset.

Temperature has a significant effect on the Sr isotope ratio. The reason for such variation in Sr isotope ratios with carbonization temperature is unclear, given the fact that such "radiogenic" isotope ratios are in theory insensitive to isotope fractionation but might include intra-specimen variability (see Section 4.2) or a minute amount of contamination during some of the experiments, for example, by ambient dust. In any case, this temperature effect was weak relative to the offset between the calcareous and acidic sites, indicating

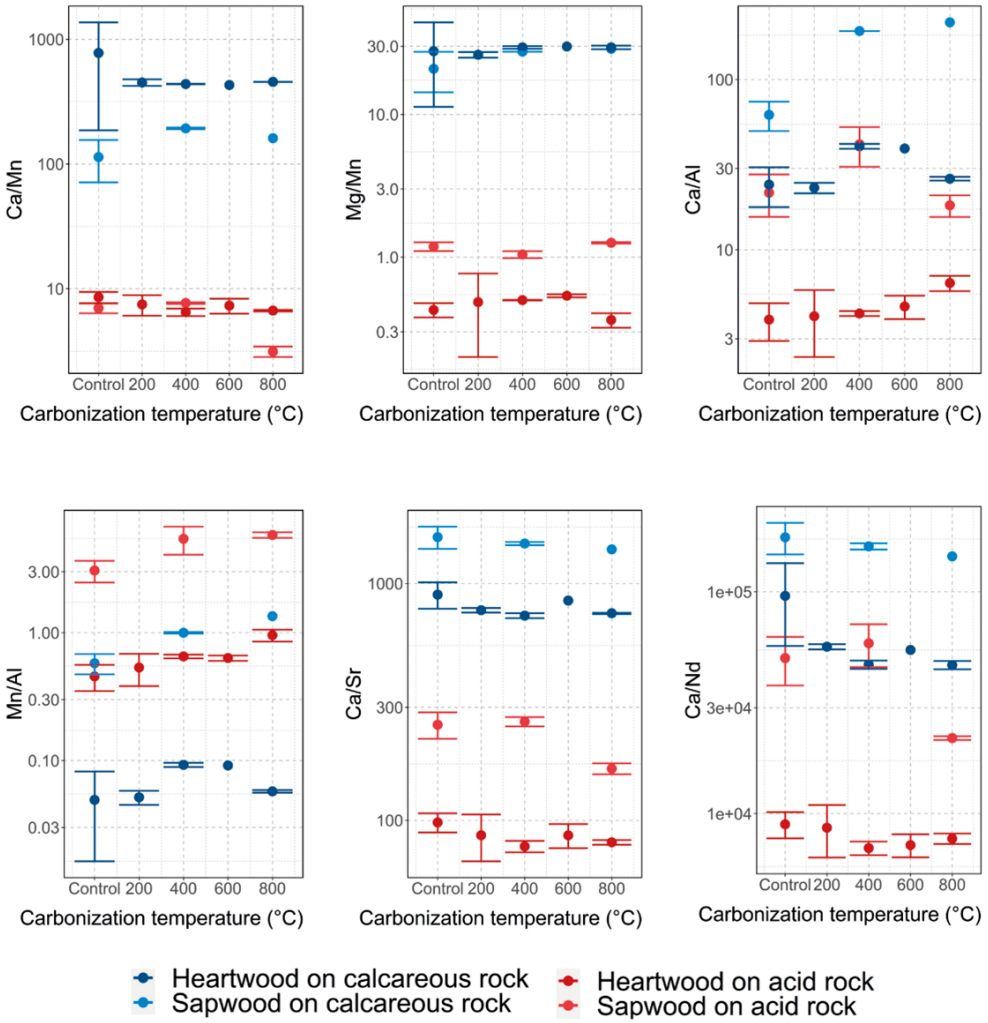

FIGURE 8 Ratios of elemental concentrations of trees from the Cagouillères site (calcareous site, blue labels) and the Bogny-sur-Meuse site (acidic site, red labels) carbonized at different temperatures. Dark shades for heartwood, light shades for sapwood. *x*-axis with log-scale

TABLE 6 Contribution (loadings) of individual elements to the linear discriminant function of site factor

Element	Ca	S	Mg	Cu	Zn	P	K	Ni	Rb	Nd	Mn	Al	Fe	Sr
Contribution	0.5	0.47	0.34	0.08	0.04	0	−0.02	−0.22	−0.23	−0.44	−0.49	−0.51	−0.53	−0.56

Ranking in order of the decreasing contribution. Elements are sorted by decreasing values of loadings.

that the variation in Sr isotopes with temperature did not interfere with the variability in site signatures (Fig. 6).

The effect of wood compartment on Sr isotope ratio was comparably strong as on the elemental ratios. Nd isotopes were not able to discriminate the provenance between the two sites. Although the use of Nd isotopes in provenancing in the specific context of this study had to be dismissed, their robustness with carbonization opens possibilities in provenance studies of charred wood, in turn calling for an optimization of measurement conditions that might improve their ability to distinguish between sites of wood origin (Section 4.3). The chemical and isotopic differentiation of heartwood and sapwood is further discussed in Section 4.2 along with the limits for wood provenancing.

4.2 *Difference between Sapwood and Heartwood*

Compared with heartwood, sapwood is generally enriched in mineral nutrients. As presented in Section 3.1, the distribution of elements was controlled more by their position relative to the boundary between physiologically active and non-active wood compartments (i.e., heartwood and sapwood) than by their distance from the pith. Nutrient accumulation within the active compartment of wood is known to be part of the tree nutrition strategy, as some of the nutrients available in the parenchyma cells of heartwood are transported towards sapwood and later remobilized in metabolic and physiological processes (Meerts 2002). Our observations are consistent with those of other studies on deciduous *Quercus* that reported enrichment in sapwood, particularly in N, Mg, P, K, Ca, and Mn (Penninckx *et al.* 2001; Durand *et al.* 2020; Figs A2 and A3 in the Appendix). In addition to the aforementioned elements, our data for sapwood indicated enrichment in S and, to a lesser extent, in Rb compared to heartwood. Supply pathways of S rely principally on soil uptake and leaf absorption of atmospheric SO_2 (Marschner 1995). Sulphur accumulation in sapwood has been reported for *Quercus robur* (de Visser 1992) and *Abies alba* (Fairchild *et al.* 2009), and Ishida *et al.* (2015) observed S-enriched sapwood in stumps of *Cryptomeria japonica* but not in living trees and deduced that the S distribution was due to translocation during heartwood formation. The S cycle in plants is complex and still poorly understood; therefore, the S pattern observed in our samples might be due to both environmental and physiological characteristics. Unlike for S, the difference in Rb concentrations between heartwood and sapwood was small. Rubidium has no known biochemical function, and its abundance in plant tissues reflects the composition of the bioavailable pool (Drobner & Tyler 1998; Taiz *et al.* 2014). Thus, it is likely that

sapwood enrichment in Rb is a side effect of K resorption, for which Rb substitutes minerals and physiological pathways.

Significant measurement uncertainty precluded any firm conclusions regarding the potential differences in Nd isotope ratios between wood compartments. The effect of wood compartment on Sr isotope ratio was comparably strong as on the elemental ratios. However, $^{87}Sr/^{86}Sr$ ratios were slightly but significantly and systematically higher in heartwood than in sapwood, which is in agreement with Rich *et al.* (2012) and Uhlig *et al.* (2020). This offset is consistent with the observed decrease in the Sr isotope ratio in tree rings from pith to sapwood in Swedish and German oaks (Åberg 1995; Maurer *et al.* 2012). These authors related the $^{87}Sr/^{86}Sr$ decrease to nutrient depletion in soils over time, leading to a higher relative contribution of lower Sr isotope ratios from atmospheric deposition to the soil. Åberg (1995) reported such a temporal decrease in mussel shells associated with an exogenous anthropogenic source. However, neither liming (Thomsen & Andreasen 2019) nor acidification (Drouet *et al.* 2005) led to a marked decrease in $^{87}Sr/^{86}Sr$ ratios at calcareous sites. Consequently, a scenario of soil nutrient depletion with time can explain the observed heartwood/sapwood difference at the acidic site of Bogny-sur-Meuse but not at the calcareous site of Cagouillères.

Instead, a possible cause for the difference in $^{87}Sr/^{86}Sr$ ratios between heartwood and sapwood could be a temporal change in rooting depth across the individual lifetime, specific to the *Quercus* tree's development (Hajj 2017). Heartwood includes rings built when trees are young, with roots accessing only shallow soil horizons, whereas sapwood is constituted at a time when roots have access to deeper soil horizons. The Sr isotope signature of the deepest soil horizons depends mostly on the bedrock, whereas the Sr isotope signature of the upper soil horizons is affected by atmospheric deposition. In bedrock with high $^{87}Sr/^{86}Sr$ ratios, the Sr isotopic signature of soil typically increases with depth, as reported by Dambrine *et al.* (1997) and Poszwa *et al.* (2003, 2004) for acidic soils developed on granitic bedrock. In contrast, a pattern of higher Sr isotope ratios in the uppermost horizons is characteristic of bedrock with low $^{87}Sr/^{86}Sr$ (Miller *et al.* 1993). Consequently, the observed difference between sapwood and heartwood for both the Cagouillères and Bogny-sur-Meuse sites could be interpreted as higher $^{87}Sr/^{86}Sr$ ratios in superficial horizons than in deep horizons. However, this explanation is unlikely given the local geological context, as the Bogny-sur-Meuse site is underlain by acidic schist rocks, for which high $^{87}Sr/^{86}Sr$ ratios are expected. However, in the absence of Sr isotope analyses of soil and rocks at the two sites, this scenario cannot be fully ruled

out. The variation in $^{87}Sr/^{86}Sr$ ratios between wood compartments was smaller than the inter-tree variation and did not hamper the identification of the site. In future studies using Sr isotopes in wood provenancing, we strongly recommend analyzing wood compartments separately instead of bulk wood.

4.3 *Difference between the Calcareous and Acidic Sites*

The elemental ratios in Fig. 8 reveal that Ca and Mg were more abundant than Mn, Sr, and Nd in wood from the calcareous site than in wood from the acidic site. Wood Ca/Mn and Mg/Mn patterns have been explained in the past by the higher bioavailability of Mn at low pH (Taiz *et al.* 2014; M. Durand *et al.* 2020), which is consistent with findings from other wood provenance studies (Kuang *et al.* 2008). It is generally accepted that Sr closely follows Ca in plants (Bowen & Dymond 1956), but selective bias may affect absorption by roots. Roca *et al.* (1995) observed a preferential uptake of Sr from soil solutions with high Ca concentrations, whereas at low Ca concentrations, the absorption rates were nearly the same. Poszwa *et al.* (2000) noted that spruces in acidified soil indicated a preferential uptake of Ca over Sr. In our study, wood Ca/Sr was more elevated at the calcareous site than at the acidic site, which is unexpected considering only the aforementioned physiological processes. To our knowledge, the Ca/Sr ratio in wood has not yet been explored for its potential in distinguishing sites of tree growth, although the proxy is familiar to archeologists working on paleodiets to infer meat *vs.* vegetal composition (Runia 1987; Sponheimer *et al.* 2005).

As expected, wood from the Cagouillères site, situated on limestone, had lower $^{87}Sr/^{86}Sr$ ratios (0.7138 ± 0.0010) than wood from the Bogny-sur-Meuse site (0.7174), which was developed on more radiogenic schists. The values measured in this study were compared with the Sr isotope ratios of plant samples indicated in the IRHUM database for metropolitan France (Willmes *et al.* 2014; 2018), available online at http://80.69.77.150/. A tree from a sampling point in the IRHUM database situated 18 km from the Bogny-sur-Meuse site had $^{87}Sr/^{86}Sr$ = 0.7123, while grass from sampling points situated respectively 11.5 and 23 km from the Cagouillères site had $^{87}Sr/^{86}Sr$ equal to 0.7108 and 0.7118. Therefore, values from the IRHUM database matched with our values acquired at the calcareous site (0.71381 ± 0.00103 for heartwood at Cagouillères; for this comparison, we considered only heartwood as the tree rooting depth during heartwood formation is more comparable with that of grass). However, there was a considerable discrepancy between the values obtained for the acidic site (0.71736 ± 0.00026 at Bogny-sur-Meuse) and the IRHUM database. This

discrepancy might be due to small-scale variability in the underlying rocks or to differences in rooting depth between trees from the two sites (Section 4.2), but these scenarios cannot be tested at this stage in the absence of further constraints on the rocks, soils, and trees from these sites.

Neodymium isotopes could not be used to distinguish between the two study sites. The first reason for this impossibility may be the similar lithological context of Nd sources. Indeed, εNd values within the range of –9 to –12 obtained in this study are typical of average detrital continental material (White 2020). In addition, minute differences that might still exist between the two sites were not detected because of the relatively poor precision obtained for Nd isotope analysis, in turn owing to the limited Nd amount available for isotope analysis. However, for future analyses, a protocol can be designed to obtain higher amounts of Nd for isotope analyses. Given the typical wood Nd concentration of tens of ppb, the minimal mass of wood prior to digestion should be 2 g to obtain an analyte sample solution containing at least 20 ng of Nd.

4.4 *Effect of Carbonization on Density Decrease and Mass Loss*

The mass loss observed with increasing temperature (Fig. 3) is typical for isothermal charring and analytical pyrolysis (Drysdale 2011). Between non-carbonized wood and wood carbonized at 200°C, the negligible mass loss is mainly attributed to the evaporation of chemically bound water (Shafizadeh 1984). The strong mass loss observed between 200 and 400°C is associated with the thermal degradation of cellulose and hemicellulose taking place from ca. 340°C to ca. 480°C (Czimczik *et al.* 2002; Yang *et al.* 2007; Nagel *et al.* 2019).

A close correlation between density and radiographic density (R^2 = 0.96) established that radiographic density as measured by the Itrax Multiscanner was as reliable as the former radiographic density methods. Both the density and radiographic density of trees A and D upturned at 600°C, but not their mass, specimen longitudinal thickness, or specimen surface in the transverse plane, which continued to decline (Fig. 3). While thickness and surface decreased constantly at a 25% rate at maximum, mass loss slowed down between 600 and 800°C, so that the mass/volume ratio became relatively higher.

Byrne *et al.* (1997) demonstrated a close linear relationship between char density and wood density (with a slope coefficient = 0.82) that is valid for various tree species, including the deciduous oak (*Quercus rubra*). In our study, the slope coefficient between the densities before and after carbonization of the trees A, B, D, and O varied between 0.47 and 0.63, with an average value of 0.55 (n = 6). Thus, the wood of *Quercus petraea* in this study underwent a

more extensive density decrease than that of Byrne *et al.* (1997). This difference might come from different experimental designs (900 vs. 800°C) and carbonization methods (no oxygen vs. minimal oxygen access).

4.5 *Effect of Carbonization on Wood Elemental Composition*

Despite the positive correlation between mineral nutrient concentrations and carbonization temperatures, the actual mass of elements in the wood decreased during our experiments (Fig. 5). Corresponding elemental mass loss was highest for S, Al, Fe, Ni, and most noticeably for Zn, which volatilized considerably between 600 and 800°C. Previous studies reported almost complete volatilization of S, Cl, and Zn and partial release of K and P at temperatures < 1000°C but diverged with respect to the behavior of other elements (Etiégni et Campbell 1991; Fagerström *et al.* 2016). The enrichment of mineral content in hardwood biochar has been documented for Mg, Mn, Al, Fe, and Na (Nagel *et al.* 2019). According to Thy *et al.* (2017), elements either volatilize during decomposition at low temperatures (250–475°C for Sc, V, Ti, Cr, Mg, and Sr) or at high temperatures (900–1300°C: for REEs, alkali metals K, Rb, Cs, and Cd, Sb, Sn). Thy *et al.* (2017) considered the differential loss between elements and did not report the initial elemental concentrations in wood, which might explain why Mg and Sr were classified as elements decomposing at low temperatures in this study. Among the elements considered weakly volatile below 800°C in Nagel *et al.* (2019) and Thy *et al.* (2017), Mg, Mn, K, and Rb were also defined as refractory elements in our study (Section 3.3). Studies dealing with pyrolysis are scarce, especially in archaeological contexts (Fermé *et al.* 2015), and it should be borne in mind that the aforementioned examples were developed for purposes of fuel pellet manufacturing from biomass and mostly in laboratory conditions different from ours (pyrolysis in a furnace with temperature control versus uncontrolled pyrolysis in muffle furnace).

5 Conclusion

Carbonization radically changes the structure and composition of the wood. The aim of this study was to verify whether and how carbonization might modify the signatures of selected geochemical markers in view of their application to charred wood provenance studies. The selected geochemical markers—elemental ratios and isotope ratios of Sr and Nd—were analysed in oak wood specimens pyrolyzed between 200 and 800°C and in a control non-carbonized specimen.

The first major finding of our study was of technical relevance: the comparison of concentration data from μ-XRF spectroscopy allowed for appraising spatial variability, and bulk ICP-MS measurements demonstrated that the former technique was capable of quantifying Mn, Ca, K, and P content in carbonized wood with satisfactory precision.

Second, our study highlighted that carbonization implied a major mass loss occurring between 200 and 400°C and continued, albeit at a lower rate, up to 800°C. Because of the mass loss related to the degradation of organic compounds, the remaining wood material became enriched in mineral components. The magnitude of the concentration increase depended primarily on the element considered and partially on the wood compartment (heartwood/sapwood).

Third, we were able to classify chemical elements based on their volatility: highly volatile elements (S and Zn), elements with intermediate thermostability (Fe, Ni, Al, and Cu), and refractory or thermostable elements (Rb, Mg, K, Nd, Sr, Mn, and Ca). This led us to propose the Ca/Mn and Mg/Mn ratios as the most appropriate elemental ratios to determine the provenance of carbonized wood because of their constancy within the entire carbonization temperature range. Other elemental markers such as Mn/Al, Ca/Sr, Ca/Nd, Ca/Al, and Ca/Fe were also rather stable throughout carbonization, but the signatures between the two study sites were less distinctive.

Fourth, our study validated the use of the Sr isotope ratio $^{87}Sr/^{86}Sr$ as a marker of charred wood origin, as the effect of carbonization on wood's $^{87}Sr/^{86}Sr$ values was weak compared to the differences between sites. The absence of any significant variation in Nd isotope ratios between different levels of carbonization indicated the reliability of this marker, although further studies should rely on higher amounts of Nd to ensure that inter-site differences can emerge from the measurement uncertainty.

Fifth, the signatures of the elemental and isotope ratios were slightly but significantly different between heartwood and sapwood, thus calling for a specific analysis of each wood compartment in wood provenance studies. We recommend focusing on heartwood to obtain a sufficient quantity of material for isotopic analysis, especially for archaeological wood, which often misses sapwood.

Providing the first framework for the variability of elemental and isotope ratios of wood within trees and through carbonization, this preliminary study suggests that the combination of these geochemical markers is a promising tool for determining the provenance of carbonized wood, which is of particular interest for samples of charred archaeological wood.

Acknowledgements

Microdensitometry and μ-XRF spectroscopy measurements were supported by SILVATECH (Silvatech, INRAE, 2018. Structural and functional analysis of tree and wood facility, doi:10.15454/1.5572400113627854E12) from UMR 1434 SILVA, 1136 IAM, 1138 BEF, and 4370 EA LERMAB Research Centre INRAE Nancy-Lorraine, for participation in. The SILVATECH facility was supported by the French National Research Agency through the Laboratory of Excellence ARBRE (ANR-11-LABX-0002-01). Sr and Nd isotope analyses were supported by the IPGP multidisciplinary program PARI and by Paris-IdF region SESAME Grant No. 12015903. The study received financial support from CNRS (MITI ISOTOP AAP 2020 – CARBONARA, 80PRIME2020), from CNRS and Ministry of Culture (MITI Chantier scientifique de Notre-Dame de Paris), and from ANR (ANR CASIMODO – ANR-20-CE03-0008). The authors would like to thank Valérie Goncalves and Laëticia Faure for help with sample preparation and assistance in laboratory. Finally, the authors are grateful to anonymous reviewers for providing insightful comments that significantly improved the clarity of the manuscript.

References

Åberg G. 1995. The use of natural strontium isotopes as Tracers in environmental studies. Water Air Soil Pollut. 79: 309–322.

Akhmetzyanov L, Allan B, Sass-Klaassen U, den Ouden J, Mohren F, Groenendijk P, García-González I. 2019. Multi-variable approach pinpoints origin of oak wood with higher precision. J. Biogeogr. 46(6): 1163–1177. DOI: 10.1111/jbi.13576.

Akhmetzyanov L, Copini P, Sass-Klaassen U, Schroeder H, de Groot GA, Laros I, Daly A. 2020a. DNA of centuries-old timber can reveal its origin. Sci. Rep. 10(1): 20316. DOI: 10.1038/s41598-020-77387-2.

Akhmetzyanov L, Sánchez-Salguero R, García-González I, Buras A, Dominguez-Delmás M, Mohren F, den Ouden J, Sass-Klaassen U. 2020b. Towards a new approach for dendroprovenancing pines in the Mediterranean Iberian Peninsula. Dendrochronologia 60: 125688.

Bayon G, Toucanne S, Skonieczny C, André L, Bermell S, *et al.* 2015. Rare earth elements and neodymium isotopes in world river sediments revisited. Geochim. Cosmochim. Acta 170: 17–38. DOI: 10.1016/j.gca.2015.08.001.

Alexander Bentley R. 2006. Strontium isotopes from the earth to the archaeological skeleton: a review. J. Archaeol. Method Theor. 13(3): 135–187. DOI: 10.1007/s10816-006-9009-x.

Boeschoten, LE, Sass-Klaassen U, Vlam M, Comans RN, Koopmans GF, *et al.* 2022. Clay and soil organic matter drive wood multi-elemental composition of a tropical tree species: Implications for timber tracing. Sci. Total Environ. 849: 157877. DOI: 10.1016/j.scitotenv.2022.157877.

Boman C, Öhman M, Nordin A. 2006. Trace element enrichment and behavior in wood pellet production and combustion processes. Energ. Fuels 20(3): 993–1000. DOI: 10.1021/ef050375b.

Boner, M, Sommer T, Erven C, Förstel H. 2007. Stable isotopes as a tool to trace back the origin of wood. Proccedinghs of the International Workshop "Fingerprinting methods for the identification of timber origins", October 8–9 2007, Bonn, Germany: 47–57.

Bowen, HJM, Dymond JA. 1956. The uptake of calcium and strontium by plants from soils and nutrient solutions. J. Exp. Bot. 7(20): 264–272.

Bridge M. 2012. Locating the origins of wood resources: A review of Dendroprovenancing. J Archaeol. Sci. 39(8): 2828–2834. DOI: 10.1016/j.jas.2012.04.028.

Byrne CE, Nagle DC. 1997. Carbonization of Wood for advanced materials applications. Carbon 35(2): 259–266. DOI: 10.1016/S0008-6223(96)00136-4.

Caro G, Bourdon B, Birck JL, Moorbath A. 2006. High-Precision 142Nd/144Nd measurements in terrestrial rocks: constraints on the early differentiation of the earth's mantle. Geochim. Cosmochim. Acta 70(1): 164–191. DOI: 10.1016/j.gca.2005.08.015.

Chen L, Wu FH, Liu TW, Chen J, Li ZJ, Pei ZM, Zheng HL. 2010. Soil acidity reconstruction based on tree ring information of a dominant species abies fabri in the subalpine forest ecosystems in southwest China. Environ Pollut. 158(10): 3219–3224. DOI: 10.1016/j.envpol.2010.07.005.

Cogez A, Meynadier L, Allègre C, Limmois D, Herman F, Gaillardet J. 2015. Constraints on the role of tectonic and climate on erosion revealed by two time series analysis of marine cores around New Zealand. Earth Planet Sci. Lett. 410: 174–185. DOI: 10.1016/j.epsl.2014.11.029.

Czimczik CI, Preston CM, Schmidt MW, Werner RA, Schulze ED. 2002. Effects of charring on mass, organic carbon, and stable carbon isotope composition of wood. Org. Geochem. 33(11): 1207–1223. DOI: 10.1016/S0146-6380(02)00137-7.

Dambrine E, Loubet M, Vega JA, Lissarague A. 1997. Localisation of mineral uptake by roots using Sr isotopes. Plant Soil. 192(1): 129–132. DOI: 10.1023/A:1004294820733.

D'Andrea R, Corona C, Poszwa A, Belingard C, Domínguez-Deláms M, *et al.* 2022. Combining conventional tree-ring measurements with wood anatomy and strontium isotope analyses enables dendroprovenancing at the local scale. SSRN. DOI: 10.2139/ssrn.4215226.

Deguilloux MF, Pemonge MH, Bertel L, Kremer A, Petit RJ. 2003. Checking the geographical origin of oak wood: molecular and statistical tools. Mol. Ecol. 12(6): 1629–1636. DOI: 10.1046/j.1365-294X.2003.01836.x.

de Visser PHB. 1992. The relations between chemical composition of oak tree rings, leaf, bark, and soil solution in a partly mixed stand. Can. J. For. Res. 22(12): 1824–1831. DOI: 10.1139/x92-238.

DeWalle, DR, Swistock BR, Sayre RG, Sharpe WE. 1991. Spatial variations of sapwood chemistry with soil acidity in Appalachian forests. J. Environ. Qual. 20(2): 486–491. DOI: 10.2134/jeq1991.00472425002000020024x.

Domínguez-Delmás M, Rich S, Traoré M, Hajj F, Poszwa A, Akhmetzyanov L, García-González I, Groenendijk P. 2020. Tree-ring chronologies, stable strontium isotopes and biochemical compounds: Towards reference datasets to provenance Iberian shipwreck timbers. J. Archaeol. Sci. Rep. 34: 102640. DOI: 10.1016/j.jasrep.2020.102640.

Doussot F, De Jéso B, Quideau S, Pardon P. 2002. Extractives content in cooperage oak wood during natural seasoning and toasting; influence of tree species, geographic location, and single-tree effects. J. Agric. Food Chem. 50(21): 5955–5961. DOI: 10.1021/jf020494e.

Drobner U, Tyler G. 1998. Conditions controlling relative uptake of potassium and rubidium by plants from soils. Plant Soil. 201: 9.

Drouet T, Herbauts J, Demaiffe D. 2005. Long-term records of strontium isotopic composition in tree rings suggest changes in forest calcium sources in the early 20th century. Glob. Change Biol. 11(11): 1926–1940. DOI: 10.1111/j.1365-2486.2005.01034.x.

Drysdale D. 2011. An Introduction to Fire Dynamics. Wiley, Chichester.

Dufraisse A, Coubray S, Girardclos O, Nocus N, Lemoine M, Dupouey JL, Marguerie D. 2018. Anthraco-Typology as a key approach to past firewood exploitation and woodland management reconstructions. Dendrological reference dataset modelling with dendro-anthracological tools. Quat. Int. 463: 232–249. DOI: 10.1016/j.quaint.2017.03.065.

Durand M, Rose C, Dupouey JL, Legout A, Ponton S. 2020. Do tree rings record changes in soil fertility? Results from a Quercus petraea fertilization trial. Sci. Total Environ. 712: 136148. DOI: 10.1016/j.scitotenv.2019.136148.

Durand SR, Shelley PH, Antweiler RC, Taylor HE. 1999. Trees, chemistry, and prehistory in the American Southwest. J. Archaeol. Sci. 26(2): 185–203. DOI: 10.1006/jasc.1998.0315.

Eckstein D, Brongers JA, Bauch J. 1975. Tree-ring research in the Netherlands. Tree-Ring Bull. 35: 1–13.

Edvardsson J, Almevik G, Lindblad L, Linderson H, Melin KM. 2021. How cultural heritage studies based on dendrochronology can be improved through two-way communication. Forests 12(8): 1047. DOI: 10.3390/f12081047.

English NB, Betancourt JL, Dean JS, Quade J. 2001. Strontium isotopes reveal distant sources of architectural timber in Chaco Canyon, New Mexico. Proc. Natl. Acad. Sci. USA 98(21): 11891–11896. DOI: 10.1073/pnas.211305498.

Etiégni L, Campbell AG. 1991. Physical and chemical characteristics of wood ash. Bioresourc. Technol. 37(2): 173–178. DOI: 10.1016/0960-8524(91)90207-Z.

Fagerström J, Steinvall E, Boström D, Boman C. 2016. Alkali transformation during single pellet combustion of soft wood and wheat straw. Fuel Process Technol. 143: 204–212. DOI: 10.1016/j.fuproc.2015.11.016.

Fairchild IJ, Loader NJ, Wynn PM, Frisia S, Thomas PA, *et al.* 2009. Sulfur fixation in wood mapped by synchrotron x-ray studies: implications for environmental archives. Environ. Sci. Technol. 43(5): 1310–1315. DOI: 10.1021/es8029297.

Fermé LC, Avilés EI, Borrero LA. 2015. Tracing Driftwood in Archaeological Contexts: Experimental Data and Anthracological Studies at the Orejas De Burro 1 Site (Patagonia, Argentina). Archaeometry. 57: 175–193.

Fowler AM, Bridge MC. 2015. Mining the British Isles oak tree-ring data set. Part A: Rationale, data, software, and proof of concept. Dendrochronologia 35: 24–33. DOI: 10.1016/j.dendro.2015.05.008.

Ganio M, Boyen S, Fenn T, Scott R, Vanhoutte S, Gimeno D, Degryse P. 2012. Roman glass across the empire: an elemental and isotopic characterization. J. Anal. Atom. Spectrom. 27(5): 743. DOI: 10.1039/c2ja10355a.

Gori Y, Wehrens R, La Porta N, Camin F. 2015. Oxygen and hydrogen stable isotope ratios of bulk needles reveal the geographic origin of Norway spruce in the European Alps. Édité par Elise Pendall. PLoS ONE 10(3): e0118941. DOI: 10.1371/journal.pone.0118941.

Gut U. 2020. Assessing site signal preservation in reference chronologies for dendro-provenancing. Édité par Adam Csank. PLoS ONE. 15(9): e0239425. DOI: 10.1371/journal.pone.0239425.

Hafner A, Reich J, Ballmer A, Bolliger M, Antolín F, Charles M, Emmenegger L, *et al.* 2021. First absolute chronologies of neolithic and bronze age settlements at lake Ohrid based on dendrochronology and radiocarbon dating. J. Archaeol. Sci. Rep. 38: 103107. DOI: 10.1016/j.jasrep.2021.103107.

Hajj F. 2017. Utilisation des isotopes stables et radiogéniques du strontium pour tracer la provenance des bois : application à des épaves sous-marines. Université de Lorraine, Nancy.

Hajj F, Poszwa A, Bouchez J, Guérold F. 2017. Radiogenic and "stable" strontium isotopes in provenance studies: a review and first results on archaeological wood from shipwrecks. J. Archaeol. Sci. 86: 24–49. DOI: 10.1016/j.jas.2017.09.005.

Haneca K, Katarina Č, Beeckman H. 2009. Oaks, tree-rings and wooden cultural heritage: a review of the main characteristics and applications of oak dendrochronology in Europe. J. Archaeol. Sci. 36(1): 1–11. DOI: 10.1016/j.jas.2008.07.005.

Harbeck M. 2011. Research potential and limitations of trace analyses of cremated remains. Forensic Sci. Int. 204: 191–200.

Hawley MF, Schroeder S, Widga CC. 2020. A Partial Charred Wooden Bowl From Aztalan (47JE1), Wisconsin. Midcont. J. Archaeol. 45(3): 306–326. DOI: 10.1080/01461109.2020.1787122.

Heier A, Evans JA, Montgomery J. 2009. The potential of carbonized grain to preserve biogenic $^{87}Sr/^{86}Sr$ signatures within the burial environment. Archaeometry 51(2): 277–291. DOI: 10.1111/j.1475-4754.2008.00409.x.

Henderson J, Evans J, Nikita K. 2009. Isotopic evidence for the primary production, provenance and trade of late bronze age glass in the Mediterranean. Mediterr. Archaeol. Archaeom. 10(1): 1–24.

Ishida T, Tayasu I, Takenaka C. 2015. Characterization of sulfur deposition over the period of industrialization in Japan using sulfur isotope ratio in Japanese cedar tree rings taken from stumps. Environ. Monit. Assess. 187(7): 459. DOI: 10.1007/s10661-015-4678-0.

Jenkins DA. 1989. Trace element geochemistry in archaeological sites. Environ. Geochem. Health 11(2): 57–62. DOI: 10.1007/BF01782994.

Kagawa A, Leavitt SW. 2010. Stable carbon isotopes of tree rings as a tool to pinpoint the geographic origin of timber. J. Wood Sci. 56(3): 175–183. DOI: 10.1007/s10086-009-1085-1086.

Kanno M, Yokoyama J, Suyama Y, Ohyama M, Itoh T, Suzuki M. 2004. Geographical distribution of two haplotypes of chloroplast DNA in Four oak species (*Quercus*) in Japan. J. Plant Res. 117(4): 311–317. DOI: 10.1007/s10265-004-0160-8.

Kassambara A, Mundt F. 2020. Factoextra: extract and visualize the results of multivariate data analyses. R Package Version 1.0.7. R Foundation for Statistical Computing, Vienna, available online at https://CRAN.R-project.org/package=factoextra.

Keppler F, Harper DB, Kalin RM, Meier-Augenstein W, Farmer N, Davis S, Schmidt HL, Brown DM, Hamilton JT. 2007. Stable hydrogen isotope ratios of lignin methoxyl groups as a paleoclimate proxy and constraint of the geographical origin of wood. New Phytol. 176(3): 600–609. DOI: 10.1111/j.1469-8137.2007.02213.x.

Krutul D, Zielenkiewicz T, Zawadzki J, Radomski A, Antczak A, Drożdżek M, Makowski TK. 2015. Non-metals accumulation in Scots Pine (*Pinus sylvestris* L.) wood and bark affected with environmental pollution. Wood Res. 60: 8.

Kuang YW, Zhou GY, Chu GW, Sun FF, Li J. 2008. Reconstruction of soil pH by dendrochemistry of Masson pine at two forested sites in the Pearl River Delta, South China. Ann. For. Sci. 65(8): 804.

Kuznetsova A, Brockhoff PB, Christensen RH. 2017. lmerTest package: tests in linear mixed effects models. J. Stat. Softw. 82(13): 1–26. DOI: 10.18637/jss.v082.i13.

Kwak JH, Lim SS, Chang SX, Lee KH, Choi WJ. 2011. Potential use of δ13C, δ15N, N concentration, and Ca/Al of Pinus densiflora tree rings in estimating historical precipitation pH. J. Soils Sediments 11: 709–721. DOI: 10.1007/s11368-011-0355-2.

Larsson M, Magnell O, Styring A, Lageråas P, Evans J. 2020. Movement of agricultural products in the Scandinavian Iron Age during the first millennium AD: $^{87}Sr/^{86}Sr$ values of archaeological crops and animals in southern Sweden. Sci. Technol. Archaeol. Res. 6(1): 96–112. DOI: 10.1080/20548923.2020.1840121.

Liepelt S, Mayland-Quellhorst E, Lahme M, Ziegenhagen B. 2010. Contrasting geographical patterns of ancient and modern genetic lineages in Mediterranean Abies species. Plant Syst. Evol. 284(3–4): 141–151. DOI: 10.1007/s00606-009-0247-8.

Lüdecke D, Ben-Shachar MS, Patil I, Waggoner P, Makowski D. 2021. Performance: An R package for assessment, comparison and testing of statistical models. J. Open Source Softw. 6(60): 31–39. DOI: 10.21105/joss.03139.

Marguerie D, Hunot JY. 2007. Charcoal analysis and dendrology: data from archaeological sites in north-western France. J. Archaeol. Sci. 34(9): 1417–1433. DOI: 10.1016/j.jas.2006.10.032.

Marschner H. 1995. Mineral nutrition of higher plants, second edn. Academic Press, London.

Maurer AF, Galer SJ, Knipper C, Beierlein L, Nunn EV, Peters D, Tütken T, Alt KW, Schöne BR. 2012. Bioavailable 87Sr/86Sr in different environmental samples – Effects of Anthropogenic contamination and implications for isoscapes in past migration studies. Sci. Total Environ. 433: 216–229. DOI: 10.1016/j.scitotenv.2012.06.046.

Meerts P. 2002. Mineral nutrient concentrations in sapwood and heartwood: a literature review. Ann. For. Sci. 59(7): 713–722. DOI: 10.1051/forest:2002059.

Miller EK, Joel D. Blum, Friedland AJ. 1993. Determination of soil exchangeable-cation loss and weathering rates using Sr isotopes. Nature 362(6419): 438–441. DOI: 10.1038/362438a0.

Million S, Eisenhauer A, Billamboz A, Rösch M, Krausse D, Nelle O. 2018. Iron Age utilization of silver fir (*Abies alba*) wood around the Heuneburg — Local origin or timber import? Quat. Int. 463: 363–375. DOI: 10.1016/j.quaint.2017.05.035.

Misra MK, Ragland KW, Baker AJ. 1993. Wood ash composition as a function of furnace temperature. Biomass Bioenerg. 4(2): 103–116. DOI: 10.1016/0961-9534(93)90032-Y.

Nagel K, Hoilett NO, Mottaleb MA, Meziani MJ, Wistrom J, Bellamy M. 2019. Physicochemical Characteristics of Biochars Derived From Corn, Hardwood, Miscanthus, and Horse Manure Biomasses. Commun. Soil Sci. Plant Anal. 50(8): 987–1002. DOI: 10.1080/00103624.2019.1594881.

Oeser RA, von Blanckenburg F. 2020. Strontium isotopes trace biological activity in the Critical Zone along a climate and vegetation gradient. Chem. Geol. 558: 119861. DOI: 10.1016/j.chemgeo.2020.119861.

Padoan M, Garzanti E, Harlavan Y, Villa IM. 2011. Tracing nile sediment sources by Sr and Nd isotope signatures (Uganda, Ethiopia, Sudan). Geochim. Cosmochim. Acta 75(12): 3627–3644. DOI: 10.1016/j.gca.2011.03.042.

Penninckx V, Glineur S, Gruber W, Herbauts J, Meerts P. 2001. Radial Variations in wood mineral element concentrations: a comparison of beech and pedunculate oak from the Belgian Ardennes. Ann. For. Sci. 58(3): 253–260. DOI: 10.1051/forest:2001124.

Pinta É, Pacheco-Forés SI, Wallace EP, Knudson KJ. 2021. Provenancing wood used in the Norse Greenlandic settlements: A biogeochemical study using hydrogen, oxygen, and strontium isotopes. J. Archaeol. Sci. 131: 105407. DOI: 10.1016/j.jas.2021.105407.

Poszwa A, Dambrine E, Pollier B, Atteia O. 2000. A comparison between Ca and Sr cycling in forest ecosystems. Plant Soil 225: 299–310.

Poszwa A, Wickman T, Dambrine E, Ferry B, Dupouey JL, Helle G, Schleser G, Breda N. 2003. A retrospective isotopic study of spruce decline in the Vosges mountains (France). Water, Air Soil Pollut: Focus 3(1): 201–222. DOI: 10.1023/A:1022176025379.

Poszwa A, Ferry, Dambrine E, Pollier B, Wickman T, Loubet M, Bishop K. 2004. Variations of bioavailable Sr concentration and 87Sr/86Sr ratio in boreal forest ecosystems. Biogeochemistry 67(1): 1–20. DOI: 10.1023/B:BIOG.0000015162.12857.3e.

Prida A, Puech JL. 2006. Influence of geographical origin and botanical species on the content of extractives in American, French, and East European oak woods. J. Agric. Food Chem. 54(21): 8115–8126. DOI: 10.1021/jf0616098.

Reynolds AC, Betancourt JL, Quade J, Patchett PJ, Dean JS, Stein J. 2005. 87Sr/86Sr sourcing of ponderosa pine used in Anasazi great house construction at Chaco Canyon, New Mexico. J. Archaeol. Sci. 32(7): 1061–1075. DOI: 10.1016/j.jas.2005.01.016.

Rich S, Manning SW, Degryse P, Vanhaecke F, Latruwe K, Van Lerberghe K. 2016. To put a cedar ship in a bottle: dendroprovenancing three ancient East Mediterranean watercraft with the 87Sr/86Sr isotope ratio. J. Archaeol. Sci. Rep. 9: 514–521. DOI: 10.1016/j.jasrep.2016.08.034.

Rich S, Manning SW, Degryse P, Vanhaecke F, Van Lerberghe K. 2012. Strontium isotopic and tree-ring signatures of Cedrus brevifolia in Cyprus. J. Anal. At. Spectrom. 27(5): 796. DOI: 10.1039/c2ja10345a.

Roca MC, Vallejo VR. 1995. Effect of soil potassium and calcium on caesium and strontium uptake by plant roots. J. Environ. Radioact. 28(2): 141–159.

Runia LT. 1987. Strontium and calcium distribution in plants: effect on palaeodietary studies. J. Archaeol. Sci. 14(6): 599–608. DOI: 10.1016/0305-4403(87)90078-1.

Ryan SE, Dabrowski V, Dapoigny A, Gauthier C, Douville E, *et al.* 2021. Strontium isotope evidence for a trade network between southeastern Arabia and India during Antiquity. Sci. Rep. 11(1): 303. DOI: 10.1038/s41598-020-79675–3.

Sandak A, Sandak J, Negri M. 2011. Relationship between Near-Infrared (NIR) Spectra and the geographical provenance of timber. Wood Sci. Technol 45(1): 35–48. DOI: 10.1007/s00226-010-0313-y.

Shafizadeh F. 1984. The chemistry of pyrolysis and combustion. Adv. Chem. 207: 489–529. DOI: 10.1021/ba-1984-0207.ch013.

Slovak NM, Paytan A. 2012. Applications of Sr Isotopes in Archaeology. In M Baskaran (ed.) Handbook of Environmental Isotope Geochemistry: 743–768. Springer, Heidelberg. DOI: 10.1007/978-3-642-10637-8_35.

Snoeck C, Lee-Thorp J, Schulting R, de Jong J, Debouge W, Mattielli N. 2015. Calcined bone provides a reliable substrate for strontium isotope ratios as shown by an enrichment experiment: strontium isotope ratios in calcined bone. Rapid Commun. Mass Spectrom. 29(1): 107–114. DOI: 10.1002/rcm.7078.

Sponheimer M, de Ruiter D, Lee-Thorp J, Spath S. 2005. Sr/Ca and early hominin diets revisited: new data from modern and fossil tooth enamel. J. Human Evol. 48(2): 147–156. DOI: 10.1016/j.jhevol.2004.09.003.

Taiz L, Zeiger E, Møller IM, Murphy A. 2014. Plant physiology and development. 6th edition. Sinauer Associates Sunderland, MA.

Thomsen E, Andreasen R. 2019. Agricultural lime disturbs natural strontium isotope variations: Implications for provenance and migration studies. Sci. Adv. 5(3): eaav8083. DOI: 10.1126/sciadv.aav8083.

Thy P, Barfod GH, Cole AM, Brown EL, Jenkins BM, Lesher CE. 2017. Trace metal release during wood pyrolysis. Fuel 203: 548–556. DOI: 10.1016/j.fuel.2017.04.050.

Towner RH. 2002. Archeological dendrochronology in the southwestern United States. Evol. Anthropol. Issues News Rev. 11(2): 68–84. DOI: 10.1002/evan.10009.

Traoré M, Kaal J, Cortizas AM. 2018. Differentiation between pine woods according to species and growing location using FTIR-ATR. Wood Sci. Technol 52(2): 487–504. DOI: 10.1007/s00226-017-0967-9.

Uhlig D, Amelung W, Von Blanckenburg F. 2020. Mineral nutrients sourced in deep regolith sustain long-term nutrition of mountainous temperate forest ecosystems. Glob. Biogeochem. Cycles 34(9): e2019GB006513. DOI: 10.1029/2019GB006513.

White WM. 2020. Chapter 7: Trace Elements. In Geochemistry, 216–313. Wiley-Blackwell.

Willmes M, McMorrow L, Kinsley L, Armstrong R, Aubert M, Eggins S, Falguères C, Maureille B, Moffat I, Grün R. 2014. The IRHUM (Isotopic Reconstruction of Human Migration) Database & ndash; Bioavailable Strontium Isotope Ratios for Geochemical Fingerprinting in France. Earth Syst. Sci. Data. 6(1): 117–122. DOI: 10.5194/essd-6-117-2014.

Willmes M, Bataille CP, James HF, Moffat I, McMorrow L, Kinsley L, Armstrong RA, Eggins S, Grün R. 2018. Mapping of bioavailable strontium isotope ratios in France for archaeological provenance studies. Appl. Geochem. 90: 75–86. DOI: 10.1016/j.apgeochem.2017.12.025.

Yang H, Yan R, Chen H, Lee DH, Zheng C. 2007. Characteristics of hemicellulose, cellulose and lignin pyrolysis. Fuel 86(12–13): 1781–1788. DOI: 10.1016/j.fuel.2006.12.013.

Young GHF, Loader NJ, McCarroll D, Bale RJ, Demmler JC, *et al.* 2015. Oxygen stable isotope ratios from British oak tree-rings provide a strong and consistent record of past changes in summer rainfall. Clim. Dyn. 45(11–12): 3609–3622. DOI: 10.1007/s00382-015-2559-4.

Appendix

A1 *Material and Methods*

A1.1 Sample Preparation for Isotope Composition Measurement

Sr concentration in procedural blanks ranged from 0.03 μg/l to 0.08 μg/l with mean ±SD of 0.05 ± 0.01 μg/l (n = 26), corresponding to a contribution of the order of a percent (0.6–1.6%) of total Sr from samples. Nd concentration in procedural blanks ranged from 0.4 ng/l to 1.3 ng/l, with a mean ±SD of 0.6 ± 0.2 ng/l (n = 26), corresponding to a contribution of the order of a percent (0.24–1.6%) of total Nd from samples. The Sr and Nd concentrations in procedural blanks that were digested were ten times higher than in non-digested blanks, which contained 0.0043 μg/l of Sr and 0.03 ng/l of Nd (n = 3 for both). Milli-Q water used to rinse digestion tubes contained 0.06 μg/l of Sr and 0.4 ng/l Nd (n = 3 for both), which was considerably higher than 2% acidified Milli-Q water (HNO_3; 0.001 μg/l for Sr and 0.03 ng/l for Nd). Therefore, we considered contamination to originate from both residuals in the digestion tubes that were not washed out and the digestion process itself.

The accuracy and reproducibility of isotope ratio measurements were assessed by standard reference materials NIST-987 for Sr (99.9 ± 0.00215%, n = 5, 2 SD = 1.53×10^{-5}) and NIST-3135a for Nd (99.9 ± 0.00694%, n = 3, 2 SD = 5.84×10^{-5}). The mass of Nd available per sample for isotope analysis was 6.7 ± 3.4 ng. Although this amount is sufficient for reliable isotope analysis, for some samples, low separation yields result in very small signals during mass spectrometry measurements.

A1.2 Comparison between ICP-MS and μ-XRF Spectroscopy

The elemental compositions were expected to correlate between the two analytical techniques. However, μ-XRF spectroscopy measurements were not calibrated because of the lack of an equivalent reference material (charred wood), and comparison with ICP-MS was instructive regarding the matrix effect. Contrary to ICP-MS, μ-XRF spectroscopy is a semi-quantitative technique, and some discrepancies in concentration measurements by the two methods were perceived here (e.g., significance of tree effect in Tables 2 and 4). In this study, the highest intensity of μ-XRF signal was recorded for K in 800°C-carbonized wood (10^6 arbitrary units a.u.), and the lowest for Ti in non-carbonized wood (10^{-1} a.u.). The correlation tests between arbitrary units from μ-XRF spectroscopy and absolute concentrations from ICP-MS indicated a generally significant (p-value < 0.05 for all elements except Ni) and a positive correlation, particularly strong for elements Mn, K, Ca, and P (Table A2). Measurement accuracy for these four elements does not seem to be impacted by carbonization.

A linear model between relative and absolute concentrations was constructed for each element from 20 common samples (Table 1). The effect of the absolute concentration was significant for elements with a high correlation coefficient (Table A3). The temperature effect was significant for Mn, K, P, Al, and S and it was indeed the only variables explaining the relative concentrations of S and Al (together with heartwood/sapwood for Al). The heartwood/sapwood effect was the most striking for Mn, which agreed with the Mn distribution described above. Interactions between variables were noticeable only for elements with a significant effect on the absolute concentration. As a result, the quality of concentration prediction based on arbitrary μ-XRF units was primarily determined by the element under consideration. Elements in this study might have been classified as (a) accurately measured elements such as Mn, Ca, K, and P; (b) elements with poor quality of measurement (Ni, Fe, Al); and (c) S, whose quality of measurement depended strongly on the carbonization state of wood. Therefore, the results obtained from relative concentrations should be considered reliable for Mn, Ca, K, and P, and with precaution for the other elements.

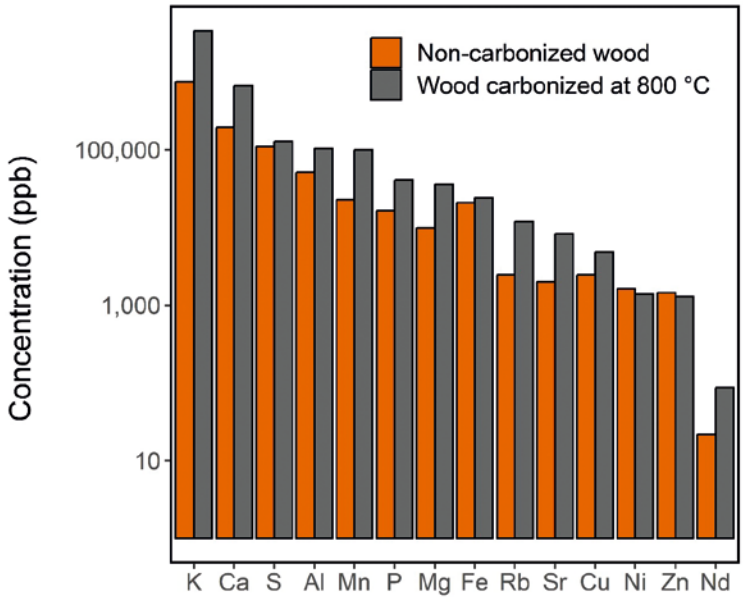

FIGURE A1 Concentration of mineral nutrients in heartwood of the tree O from the acidic site Bogny-sur-Meuse, with log-scale for the *y*-axis. Brown bars indicate non-carbonized wood, and gray bars indicate wood carbonized at 800°C. Elements are sorted along the *x*-axis by decreasing values of concentration in non-carbonized wood.

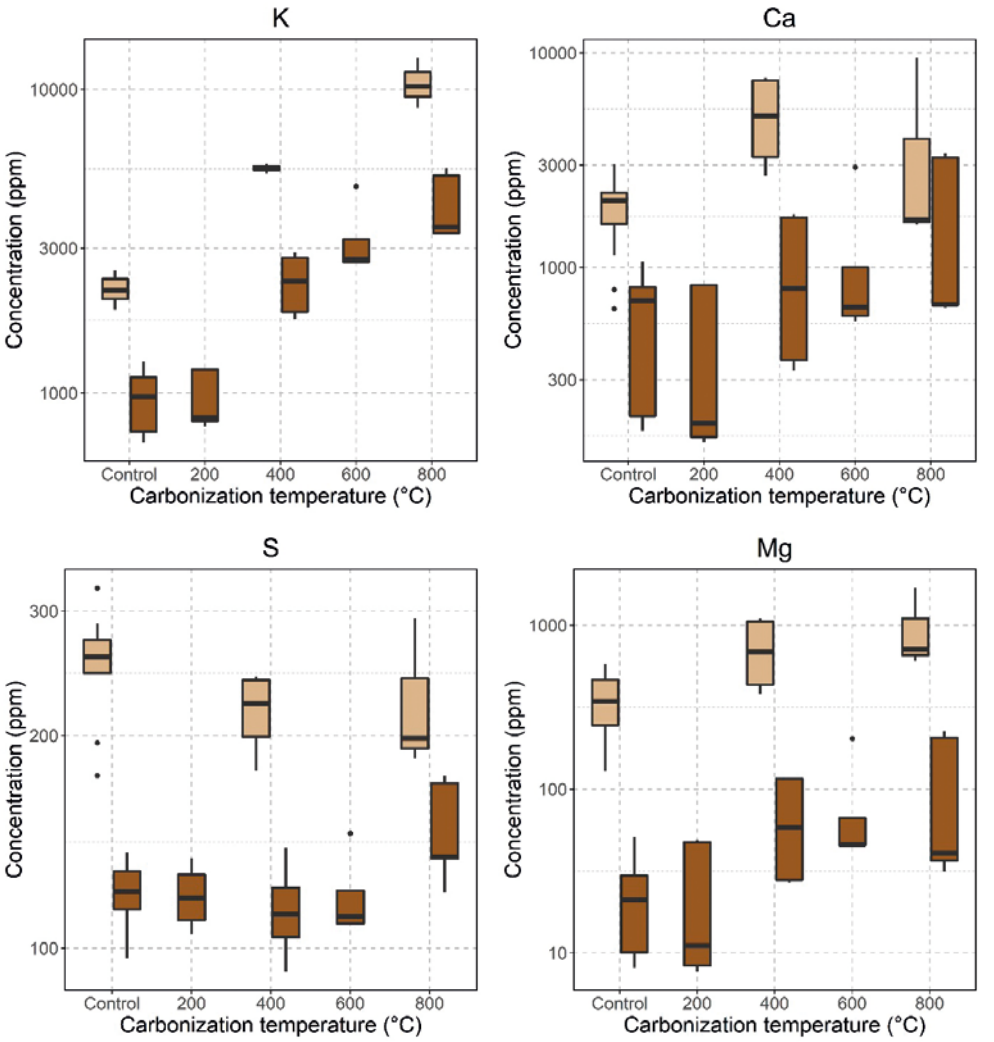

FIGURE A2 Bulk concentrations (n = 4, including trees from both calcareous and acidic substrates) from ICP-MS in heartwood (dark brown) and sapwood (light brown) of wood specimens carbonized at different temperatures. Box plots show the median, first, and second quartiles.

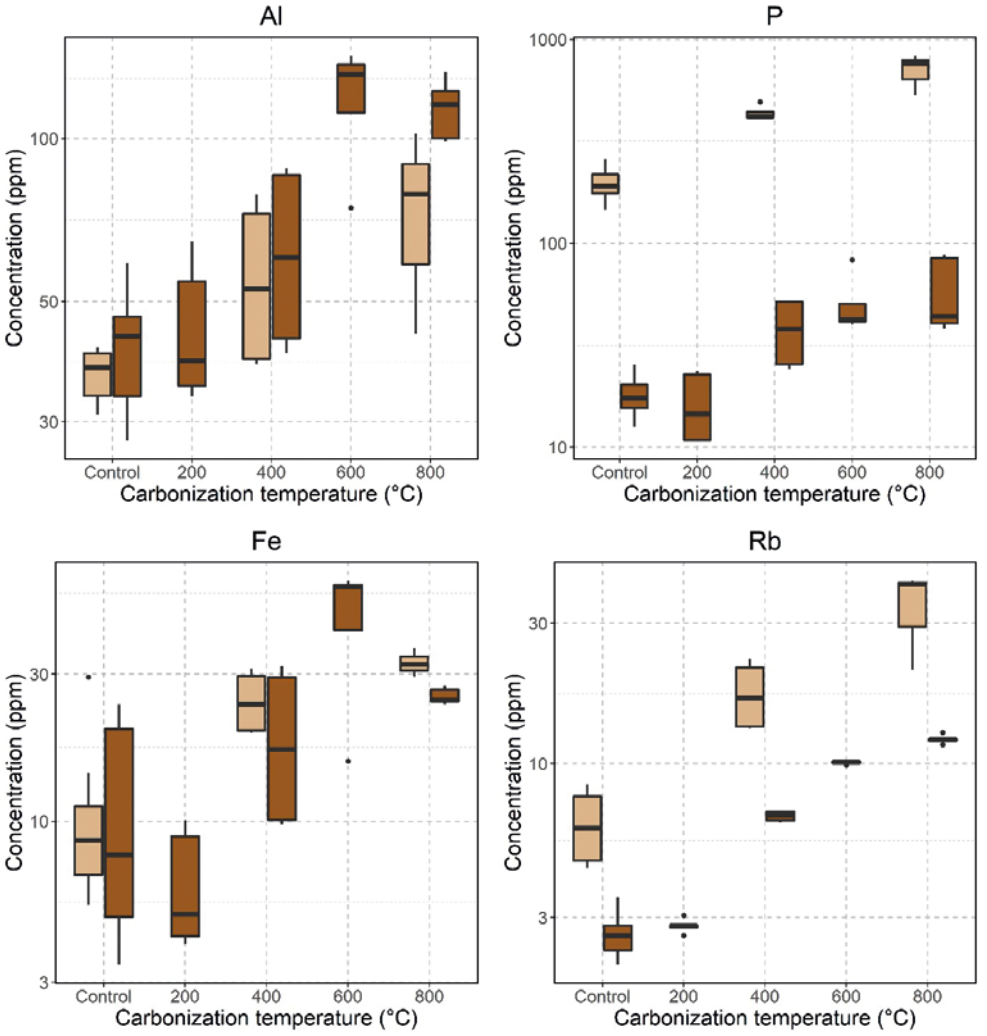

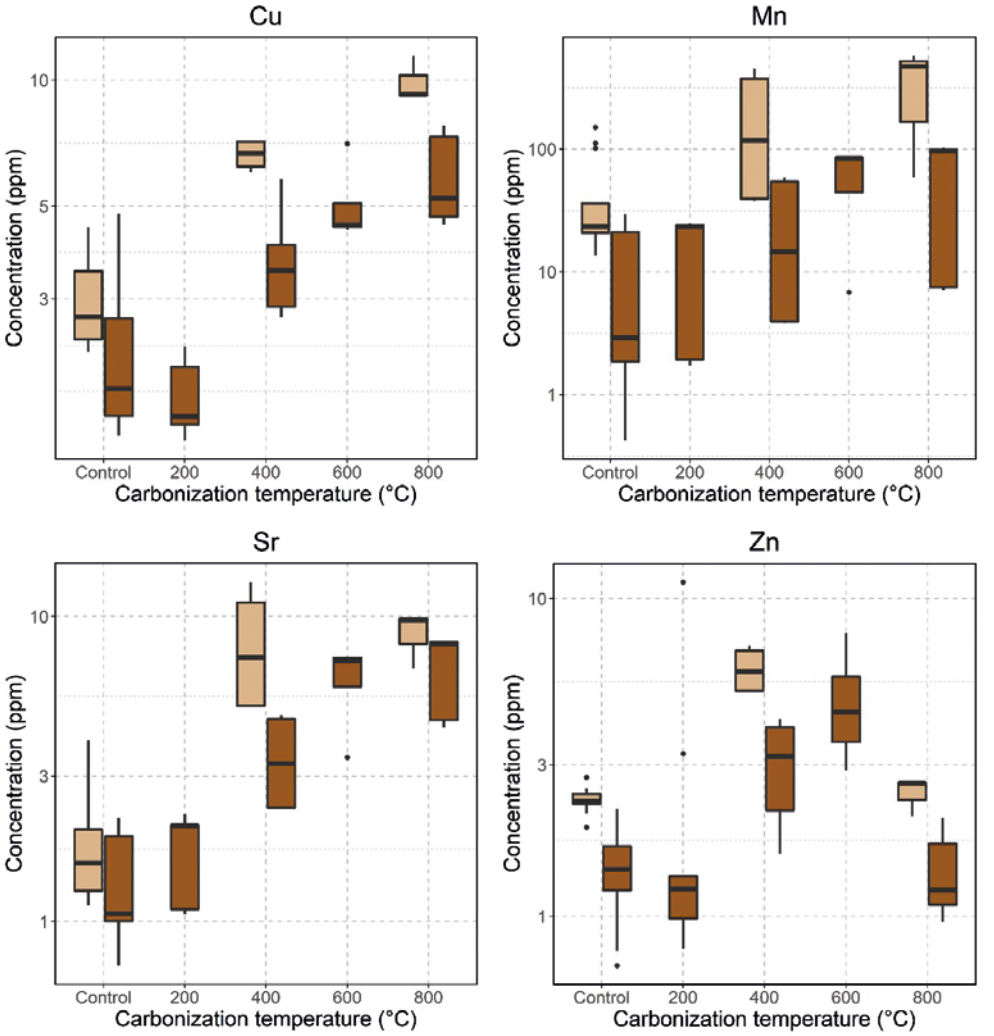

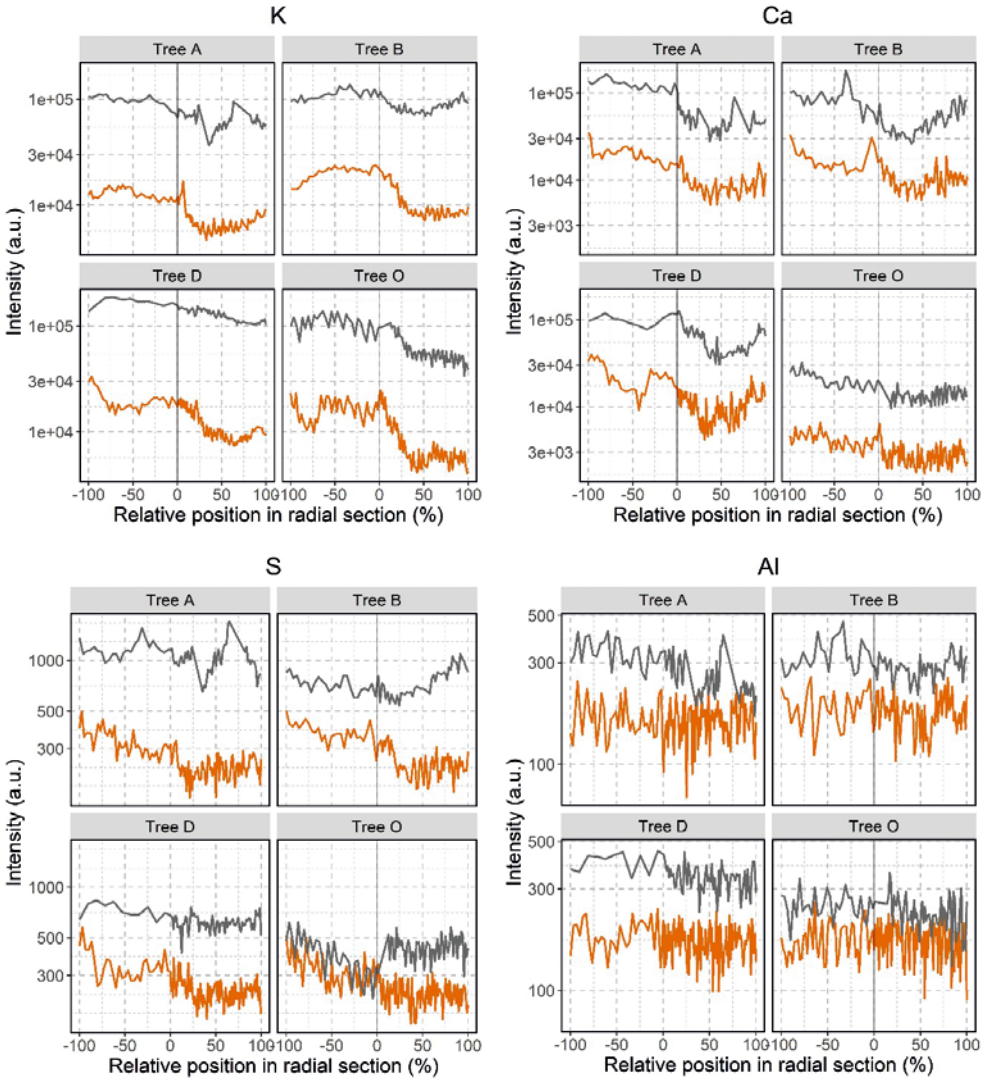

FIGURE A3 Intensity of μ-XRF signal in arbitrary units measured per point along the radial section of the wood specimens, with results for non-carbonized wood in brown and wood carbonized at 800°C in grey. "0" on the *X*-axis corresponds to the heartwood/sapwood boundary; values are negative in the sapwood section and positive in the heartwood section.

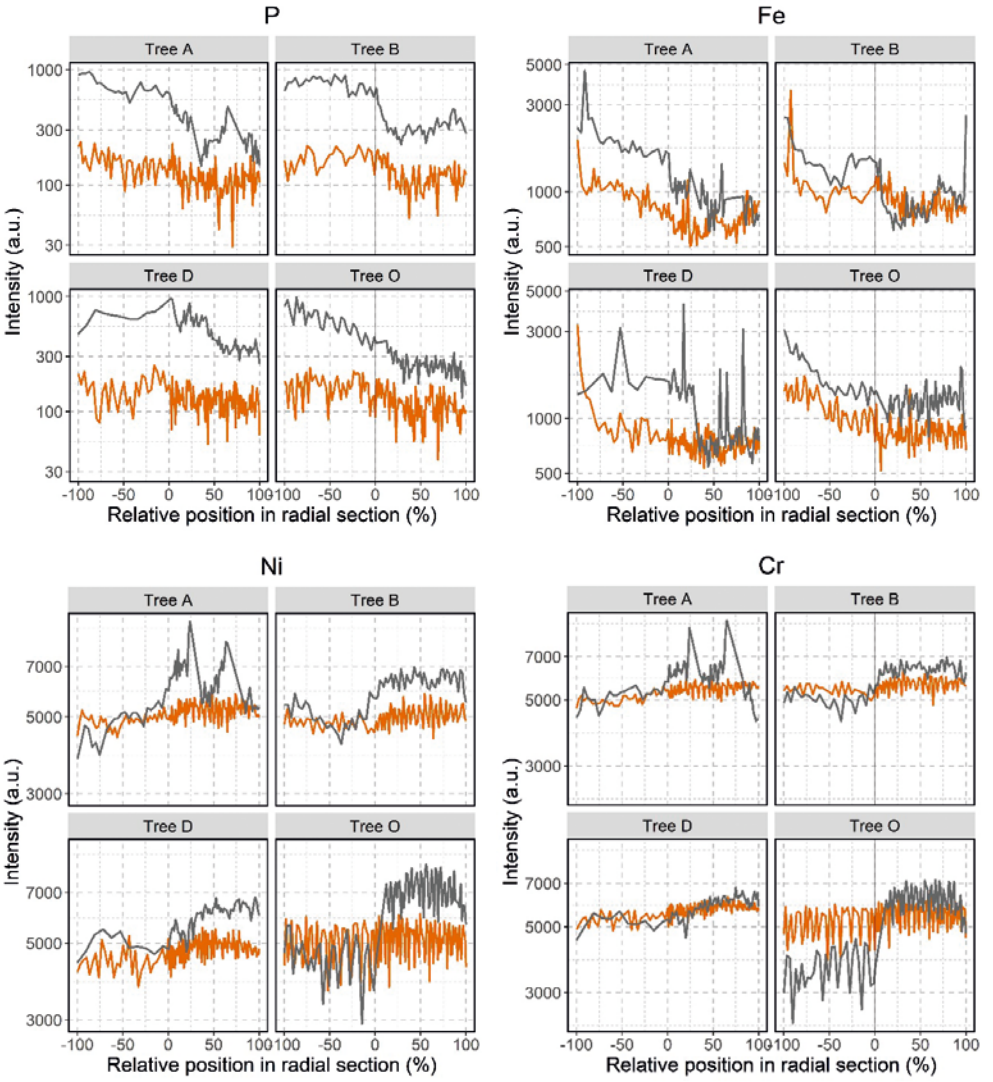

TABLE A1 Accuracy in % (n = 10, RSD) estimated for standard reference material INCT-OBTL-5 and contamination rate for blanks (n = 20, RSD)

Element	Accuracy ± RSD (%)	Contamination rate (%)
Rb	97.3 ± 3.2	1.22 ± 0.23
Sr	102.4 ± 4.0	1.32 ± 0.25
Nd	95.8 ± 4.0	1.19 ± 0.33
Mg	105.5 ± 7.91	1.11 ± 1.59
Al	84.8 ± 5.9	12.43 ± 1.93
P	117.8 ± 9.0	1.86 ± 1.62
S	117.6 ± 10.5	0.52 ± 0.77
K	101.74 ± 6.29	0.23 ± 0.23
Ca	123.88 ± 8.44	1.48 ± 0.52
Mn	105.6 ± 5.5	0.04 ± 0.04
Ni	116.6 ± 11.2	1.20 ± 1.33
Cu	113.0 ± 6.3	0.60 ± 0.35
Zn	111.2 ± 4.5	4.76 ± 4.08

TABLE A2 Correlation (n = 20) between relative concentration in a.u. from μ-XRF spectroscopy and absolute concentration in ppm from ICP-MS

Element	Pearson's correlation	Spearman's correlation	Pearson's correlation of log of concentration
Mn	0.99***	0.98***	0.93***
K	0.93***	0.94***	0.96***
Ca	0.88***	0.87***	0.91***
P	0.83***	0.79***	0.77***
Fe		0.63**	0.63**
Al		0.63***	0.60***
S	0.5*	0.61**	0.58**
Ni			

*** p < 0.001, ** p = 0.001–0.01, * p = 0.01–0.05, otherwise blank. Correlation coefficient r of Spearman's and Pearson's correlation (for concentrations and for log of concentrations) presented for p < 0.05. Elements are sorted by decreasing values of Pearson's r.

TABLE A3 ANOVA statistics of model of μ-XRF spectroscopy measurements

Element	Conc.	Comp.	Temp.	Conc.* Comp.	Conc. * Temp.	Comp. * Temp.	Conc. * Comp. * Temp.	R^2
Mn	55630.51***	434.05***	56.99***	1095.78***	240.25***			1
K	23.51***	6.57*	14.99***	15.83***	24.74***		15.43***	0.99
Ca	125.51***	5.32*	3.18	18.66***	0.95			0.96
P	41.48***		14.76***			5.09*	7.04***	0.98
Fe								0.75
Al		6.17*	56.91***					0.91
S	4.95*		36.99***					0.9
Ni								0.67

*** $p < 0.001$, ** $p = 0.001–0.01$, * $p = 0.01–0.05$, otherwise blank. *F*-values presented for $p < 0.05$. Elements sorted in decreasing order of correlation coefficient (not presented here). Conc., absolute ICP-MS concentration; Comp., wood compartment; Temp., temperature.

TABLE A4 AIC scores of models of μ-XRF relative concentrations as a function of ICP-MS absolute concentration, with Model 3 selected as the most appropriate

Element	Model 1	Model 2	Model 3	Model 4	Model 5
Al	202.13	178.83	172.63	179.73	162.79
S	224.69	204.39	198.71	209.95	177.45
P	232.74	204.16	189.50	200.16	192.01
Fe	261.45	265.25	257.56	268.45	213.57
Mn	317.41	316.60	230.48	253.03	227.60
Ni	295.61	296.61	288.44	294.92	262.88
Ca	382.54	380.10	361.48	340.93	299.38
K	395.84	384.53	363.86	384.68	341.68

XRF, μ-XRF relative concentration; ICP, ICP-MS absolute concentration; Temp., temperature. Model 1: XRF ~ ICP; Model 2: XRF ~ ICP * Temp.; Model 3: XRF ~ ICP * Temp. * Wood compartment; Model 4: XRF ~ ICP * Temp. * Site; Model 5: XRF ~ ICP * Temp. * Wood compartment * Site.